Theses and Dissertations   Graduate School

2013

Atomic and Electronic Structure of a Ligand-Protected Bimetallic Nanocluster, Ag4Ni2(DMSA)4

Anthony F. Pedicini
Virginia Commonwealth University

www.manaraa.com

ATOMIC AND ELECTRONIC STRUCTURE OF A LIGAND-PROTECTED BIMETALLIC
NANOCLUSTER, Ag_4Ni_2 (DMSA)$_4$

A thesis submitted in partial fulfillment of the requirements for the degree of

Master of Science in Physics/Applied Physics at Virginia Commonwealth University

by

ANTHONY FILIPPO PEDICINI

B.S. in Physics
B.S. in Applied Mathematics

Virginia Commonwealth University, 2011

M.S. in Physics

Virginia Commonwealth University, 2013

Director: SHIV N. KHANNA, Ph.D.

COMMONWEALTH PROFESSOR, DEPARTMENT OF PHYSICS

Virginia Commonwealth University

Richmond, Virginia

May, 2013

Acknowledgements

At the outset I would like to thank Dr. Shiv N. Khanna for accepting me into his research group and for his advisement and tutelage throughout the past two years. His experience, extensive knowledge, and dedication have made for a great learning environment. I would like to thank the entirety of the Khanna Research Group, with special recognition to Dr. Arthur Reber. Art has taken a portion of his valuable time to both answer questions and impart knowledge I would not have learned elsewhere.

Table of Contents

Table of Contents (Cont.)

List of Figures

List of Figures (cont.)

List of Figures (Cont.)

List of Figures (Cont.)

Abstract

ATOMIC & ELECTRONIC STRUCTURE OF A LIGAND-PROTECTED BIMETALLIC NANOCLUSTER, Ag_4Ni_2 $(DMSA)_4$

By ANTHONY FILIPPO PEDICINI

A thesis submitted in partial fulfillment of the requirements for the degree of Master of Science in Physics/Applied Physics at Virginia Commonwealth University.

Virginia Commonwealth University, 2013.

Major Director: Shiv N. Khanna, Ph.D., Commonwealth Professor, Department of Physics

An important direction in nanoscale science is to synthesize materials whereby atomic clusters serve as the building blocks. Properties of these clusters can be controlled through size and composition, and such an approach offers a pathway toward designing larger, customized materials. One way to stabilize such materials is through the use of ligated clusters. $Ag_4Ni_2(DMSA)_4$ is one such cluster, the first with a bimetallic core, and has been stabilized by the experimental group of A. Sen at The Pennsylvania State University. The theoretical studies undertaken in this thesis were directed toward providing information on the atomic structure, nature of electronic states, optical spectra, and any magnetic information of this new species. Theoretical studies have also been carried out on various clusters to provide input into the fragmentation data obtained through MS/MS experiments.

Chapter 1. Introduction

1.1 Background & Motivation

The macroscopic world in which we live is a familiar one to us now, and long gone are the days in which everyday objects excite and entrance us. Few of us go further into learning the composition of these items, to delve into the basic building blocks of matter. But, it is here, in the atomic world, in which the adventure of miniaturization and customization of materials begins. This atomic world ranges from few to a few hundred, and even thousands of atoms and stands as the meeting ground for numerous branches of science. This meeting ground is also the starting place for a new branch, nanoscience, where new physical properties of matter are found thanks to the effects of quantum mechanics. But, one does not simply venture into new areas of science by accident. The journey of nanoscience began a very long time ago, and has been the eventual merger of chemistry, physics, materials science, biology, and medicine, linking each other together at the most fundamental level.

One can imagine the scope in which this area entails. Chemistry and physics joining together to move beyond understanding the basic elements and their interactions with each other, to using this information garnered from years of investigation to control them for our personal gain. Beginning with an element out of the periodic table, up to and through to its natural function and form, to now, customizing new functionality within specialized structures. The

chosen element (and sometimes elements) immediately dictates the direction in which one moves forward in creation of a nanosized object. Arrangement of these atoms and their subsequent geometry will determine all of that clusters physical properties, i.e. optical, magnetic, mechanical, and in many cases, reactivity. It is because of the numerous bonding options available to us when using a solitary atom that affords us the ability to place them wherever desired and needed. The possible combinations can seem endless and are made more complex when it has become possible to take these clusters and form new three dimensional solids, Cluster-Assembled Materials.[1,2]

The versatility of clusters has long been established, and goes unbeknownst to many. This versatility has taken nanoscience into the realm of nanotechnology. Nanotechnology (in the sense of its current popularization, rather than Atomically Precise Manufacturing (APM)) in the everyday is not only found in the obvious sources of technology, i.e. computers and cellular phones. (Two of the many things which have a lineage that started at a size which compares to their modern counterparts as monolithic.) But, into a multitude of other places, which often go unnoticed, including additives in clothing, gasoline, air filtration, etc. Nanoclusters themselves have taken on their own sub-classification system to fully describe what their use entails, and their composition. Metallic clusters, bimetallic, ligand-, and monolayer-protected just to name a few. A literature search of any combination of these terms will bring a host of various publications, all devoted to some aspect of element or elements used, variation, synthesis, growth, characterization, form, and functionality.

Building nanostructures upwards from the atomic scale (what has been termed the "bottom-up" approach) provides us an opportunity most interesting with regard to clusters, a firsthand account of the evolution from a single atom to a nanocluster. This transformation

process is where physical properties are formed, and the heart of nanocluster science, where cluster size progression offers a gateway for tuning their stability through closing of the electronic orbitals shells. This is again derived from the choice of elements used and their possible combinations. The reduced size often leads to grouping of electronic states into orbital shells, and their filling leads to energetic stability, similar to that of atomic orbital shells. An example of shell closing can be seen in the group 18 elements of the periodic table, elements like Helium, Neon, and Argon. It is this shell closing idea that allows us to combine elements to our hearts desire and still have a stable product in the end. With this in mind, the motivation is clear, to formulate and construct new and unseen cluster forms. To which, through combining multiple properties such as magnetism, size, and shape, can offer new areas of nanocluster science and broaden an already widening field to encompass all varieties and combinations.

The purpose of this investigation was to take a ligand protected nanocluster with pure silver metal core and introduce nickel, in an effort to combine a few of the aforementioned properties, and further the understanding of bimetallic cluster cores as it is still a relatively new area. The addition of Nickel would offer the cluster a possible mechanism through which magnetic behavior could be acquired. Magnetism is indicated by an excess of spin-up electrons in a given cluster. Ferromagnetism in a system is classified as an alignment of magnetic moments, each centered on two atoms. If these magnetic moments are coupled opposite directions, this then creates an anti-ferromagnetic system. In either case the successful addition of Nickel, if ferromagnetic, anti-ferromagnetic, or neither, introduces a new type of ligand-protected cluster, one with a bimetallic core. This is not the first bimetallic ligand-protected cluster, but it is perhaps the first to consist of a noble-metal and a transition metal from the first row of the periodic table.[24] The added benefit of this cluster and its metallic cored counter parts

is that they can be synthesized if need be in macroscale quantities, few to tens or even hundreds of kilograms.

In addition to atomic structure, the theoretical studies should provide for an understanding of the observed optical spectra and information regarding the magnetic nature of the cluster material. We have undertaken studies into the atomic & electronic properties using first principles electronic structure methods. We outline these methods in chapter 2 which are the essentials of the theoretical approach. Subsequently, in chapter 3 the discussion of our results and findings based on the $Ag_4Ni_2(DMSA)_4$ cluster are elaborated. Next, chapter 4 outlines the findings due to fragmentation through electrospray mass select/mass spectrometry (MS/MS). Finally, within chapter 5 a summary of our findings and a brief outline for the future.

1.2 Experimental Procedure

The cluster material reported herein was synthesized chemically by the research group directed by Ayusman Sen at The Pennsylvania State University, University Park. In synthesis of the bimetallic cluster, the preferred route is to modify a pre-established method for that of a monometallic version.[3,4] The precursor and homo-analogue to $Ag_4Ni_2(DMSA)_4$ is the $Ag_7(DMSA)_4$ cluster (Figure 1), which has been synthesized and characterized by multiple groups since its first presentation several years ago.[5]
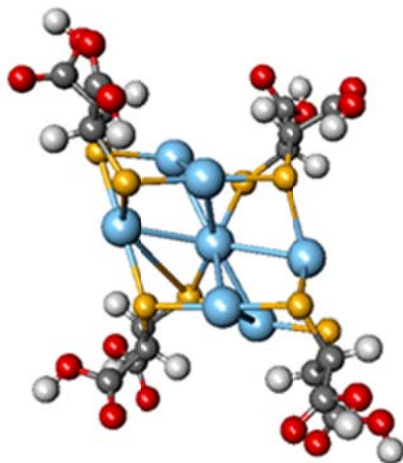
Figure 1. The ground state geometry of the $Ag_7(DMSA)_4$ cluster as calculated through DFT for use in this investigation.[6]

It is in our interest to discuss now precisely the procedure for the synthesis of $Ag_4Ni_2(DMSA)_4$. This procedure begins with the deoxygenation of ethanol through bubbling of N_2 (Nitrogen) gas. From here, a mixture of 86.6 milligrams of silver nitrate ($AgNO_3$) and 26.2 milligrams of nickel nitrate hexahydrate ($NiNO_3$) were added and allowed to dissolve within a round bottom flask. This flask was then placed in an ice bath to be cooled to 0 degrees. Once this was accomplished, the flask was opened to receive 108.0 milligrams of dimercaptosuccinic acid (DMSA). DMSA is a bi-dentate organosulfur compound most often used in chelation due to its strong bonding nature with heavy metals, such as Mercury (II) and Lead (II). DMSA (Figure 2) lends itself to this role quite nicely as it does not cross the blood-brain barrier, thus subjugating itself to extraction of metals in the entire body except the central nervous system. The use of DMSA within the body is in part due to its stability in both in air and solvents. The bonding nature has been explored through attachment to gold and zinc nanoparticles, and has served as a viable alternative to the use of other ligands, such as alkanethiols and glutathione.
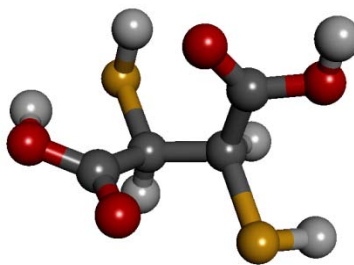
Figure 2. One of the three stereoisomers of the dimercaptosuccinic acid (DMSA) ligand.

Once the DMSA was added to the flask a yellow-green suspension formed and the system was allowed to reach equilibrium for four hours upon which time 46.5 milligrams of sodium borohydride ($NaBH_4$) in combination with 5 milliliters of ethanol (EtOH) was added and stirred vigorously. After the solution was allowed to react and reach room temperature overnight, it was subsequently centrifuged and cleaned through the use of methanol and ethanol. Any solids obtained were dried under nitrogen gas flow, dissolved in water, and centrifuged once more. Finally, the cluster was precipitated through ethanol, dried and purified through the polyacrylamide gel electrophoresis (PAGE) process (Figure 3A, Inset), yielding a green solid. This green solid is the cluster of interest, while the yellow band is that of $Ag_7(DMSA)_4^-$.
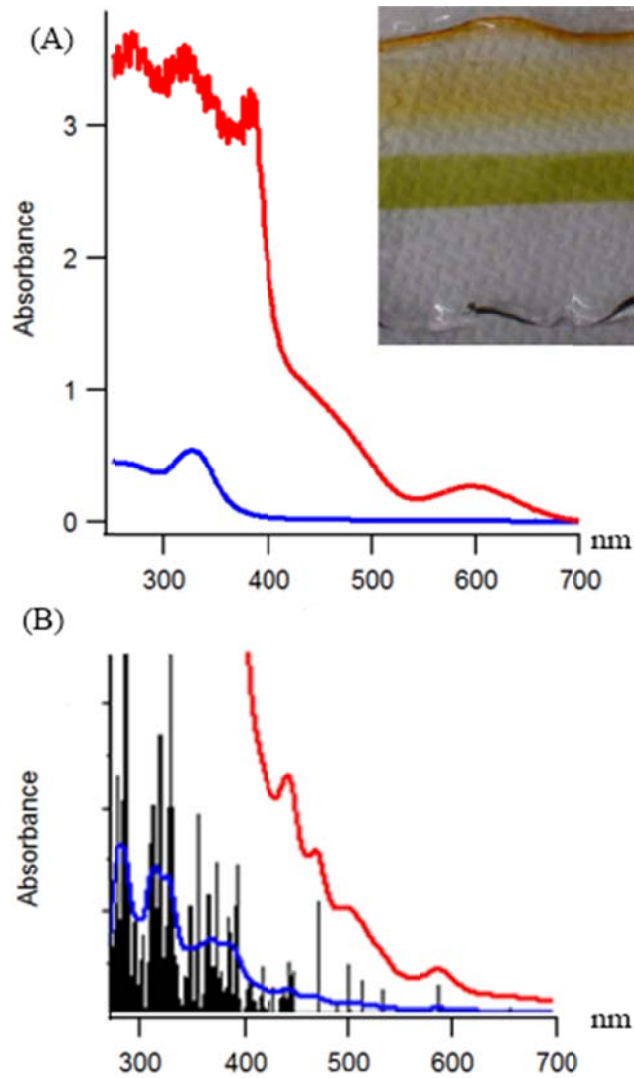
Figure 3. (A) UV-Vis experimental spectra of $Ag_4Ni_2(DMSA)_4$ in deoxygenated water. The red spectrum solution concentration was 40 times that of the blue spectrum. Inset shows the product of the PAGE procedure in separating the green $Ag_4Ni_2(DMSA)_4$ cluster. (B) Simulated UV-Vis spectra for $Ag_4Ni_2(DMSA)_4$, with red spectrum ten times that of the blue spectrum; black indicating oscillator strength. (Reproduced from [24])

The desired cluster was identified through two techniques, electrospray ionization mass spectrometry (Figure 4) and elemental analysis. Electrospray mass spectrometry is the desired method for analyzing the structure of a cluster when the crystallized form is not available, as crystallization requires the exact, isolated cluster. As such, the solid described above can only provide for the resultant optical spectra in its present state. The electrospray ionization MS/MS process displayed a cluster of mass 1269.4 amu (having the formula of $Ag_XNi_Y(DMSA)_Z$ which was the most pronounced) yielding information to assign $Ag_4Ni_2(DMSA)_4$ as the most likely candidate for the synthesized cluster.
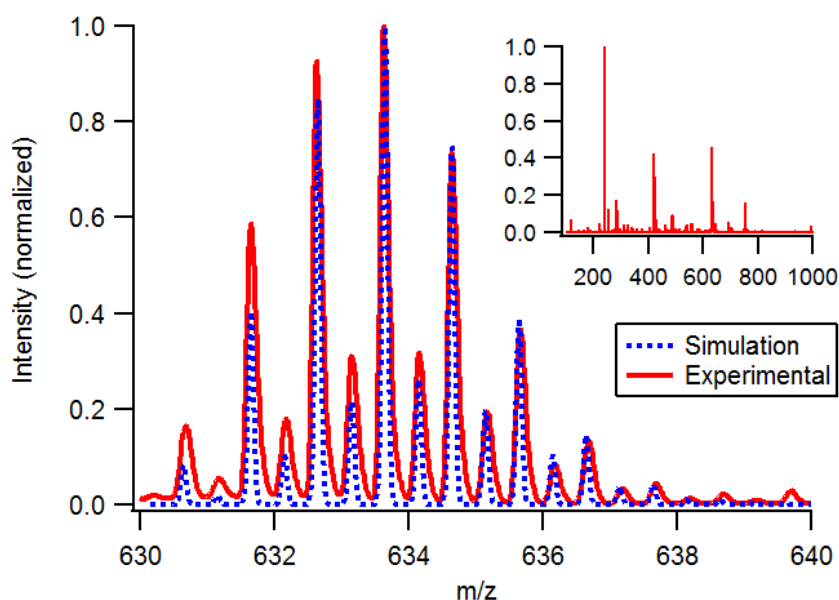
Figure 4. Mass spectrum of both experiment and simulation of the $Ag_4Ni_2(DMSA)_4$ cluster. Inset shows entire spectrum. (Reproduced from [24])

While electrospray provides for the composition of the cluster, it provides for no information regarding the arrangement of the atoms or the resulting electronic properties. The initial task of performing theoretical calculations was to identify the exact atomic structure of the cluster. As the cluster contains multiple atoms, both orientation, and conglomeration have to be

considered, as well as the multitude of combinations and geometries of the elemental

constituents themselves. These results would then be used to obtain the ground state geometries

of the fragments present within the MS/MS experiments, and also possibly provide illumination

of a synthesis path that the cluster formation has undergone.

Chapter 2. Electronic Structure Calculation

2.1 Electronic Structure Calculation in Solving the Schrödinger Equation

The quest to solve one of the central problems of quantum chemistry, the electronic problem, has been long. This problem entails describing of the motion of electrons in a group of point nuclei. The beginning of which is marked by the discovery of time-independent Schrödinger Equation and approximating its solutions,

$$\widehat{H}\left|\Psi\right\rangle = E\left|\Psi\right\rangle \tag{2.1.1}$$

where $\widehat{H}$ is the Hamiltonian operator for a system of nuclei and electrons, E, the energy, and Ψ the wavefunction. Thus, for N electrons and M nuclei, we can write the Hamiltonian as

$$\widehat{H} = -\sum_{i=1}^{N}\frac{1}{2}\nabla_i^2 - \sum_{A=1}^{M}\frac{1}{2M_A}\nabla_A^2 - \sum_{i=1}^{N}\sum_{A=1}^{M}\frac{Z_A}{r_{iA}} + \sum_{i=1}^{N}\sum_{j>i}^{N}\frac{1}{r_{ij}} + \sum_{A=1}^{M}\sum_{B>A}^{M}\frac{Z_A Z_B}{R_{AB}}, \tag{2.1.2}$$

with M_A the mass ratio of nucleus A to the mass of an electron, Z_A the atomic number of nucleus A, $\vec{R}_i$ are the positions of the nuclei, with $\vec{r}_i$ the positions of the electrons. Furthermore, $R_{AB} = \left|\vec{R}_A - \vec{R}_B\right|$ and $r_{ij} = \left|\vec{r}_i - \vec{r}_j\right|$. The Laplacians of ∇_i^2 and ∇_A^2 perform differentiation on the coordinates representing the ith electron and A^{th} nucleus. The first term of the Hamiltonian describes the kinetic energy of the electrons; the second term is the kinetic energy term of the nuclei themselves. The third term, what we shall term ν_{ext}, describes the

Coulombic attraction between nuclei and electrons, the fourth term entails the electron-electron repulsion and fifth, the nuclei-nuclei repulsion.[7]

The exact solution to (2.1.2) for a many electron system is difficult using the existing computational resources and hence it is necessary to make a few simplifications. First, taking into account the fact that the nuclei are much heavier than their electron counterparts, they respond more slowly than electrons. As such, the electrons can be considered to be in their ground state at any point in time, and the nuclei are deemed stationary. The motions of both can then be, in effect, decoupled from one another and viewed simply as electrons moving around a group of nuclei. This decoupling is called the Born-Oppenheimer Approximation, and is the first assumption in various techniques in the treatment of electrons in and around molecules. With this approximation, we can neglect the second term in (2.1.2), the kinetic energy of the nuclei, and the last term, the nuclei-nuclei repulsion, which can be considered a constant. What remains is the electronic Hamiltonian, i.e.

$$\widehat{H}_e = -\sum_{i=1}^{N} \frac{1}{2} \nabla_i^2 - \sum_{i=1}^{N} \sum_{A=1}^{M} \frac{Z_A}{r_{iA}} + \sum_{i=1}^{N} \sum_{j>i}^{N} \frac{1}{r_{ij}} . \tag{2.1.3}$$

The solution to the Schrödinger Equation that involves the electronic Hamiltonian is the wavefunction

$$\Psi_e = \Psi\left(\left\{\vec{r_i}\right\}, \left\{\vec{R_A}\right\}\right), \tag{2.1.4}$$

which depends on the position of the electrons explicitly, and only depends on the position of the nuclei simply as a parameter. One can see that each term involves three dimensions, and addition of atoms and electrons to the problem grows the expense of finding a solution.

For a system in a particular state Ψ, possibly able to satisfy (2.1.1), the average energy measurement can be found using

$$E[\Psi] = \frac{\langle \Psi | \widehat{H} | \Psi \rangle}{\langle \Psi | \Psi \rangle}, \tag{2.1.5}$$

with

$$\langle \Psi | H | \Psi \rangle = \int \Psi^* \widehat{H} \Psi d\vec{x}. \tag{2.1.6}$$

Any measurement of the energy gives an eigenvalue of $\widehat{H}$, we obtain $E[\Psi] \geq E_0$. This energy computed from an initial supposition of Ψ gives the upper bound of E_0. Minimization in its entirety, across all electron wavefunctions, will yield Ψ_0 and its energy, E_0. As such, each eigenstate of Ψ is an extremum of $E[\Psi]$ and one must replace (2.1.1) with the variational principle

$$\delta E[\Psi] = 0, \tag{2.1.7}$$

to which, solving Ψ as a function of E, then adjusting E until normalization, satisfies the Schrödinger Equation, (2.1.1). This is the basic principle and procedure for arriving at a ground state wavefunction from N electrons and a nuclear potential $v(\vec{r})$, subsequently the ground sate energy.[7,10] This variational technique is what is employed in modern calculation routines.

So far, we have only discussed the positions in space where the electrons may be found. In order to fully describe their properties, we must include spin. To do this we introduce two quantities, spin up, $\alpha(s)$, and spin down, $\beta(s)$, where both are functions of some variable s, both complete, and orthogonal to one another. Together, we can denote each electron with all its respective coordinates as $\vec{x}$,

$$\vec{x} = \{\vec{r}, s\}. \tag{2.1.8}$$

12

Thus, for an N - electron wavefunction we may write $\Psi\left(\vec{x}_1, \vec{x}_2, ..., \vec{x}_N\right)$. But, merely adding the spin component to the wavefunction does not produce anything new, as the Hamiltonian operator makes no reference to spin of any sort. Therefore, the further imposition of the requirement that the wavefunction of a many-electron system must be antisymmetric whence interchanging the coordinate $\vec{x}$, position and/or spin, of any two electrons.[7] This is called the antisymmetry principle, which is a generalized statement of the Pauli exclusion principle.

The orbital picture in which we would like to decipher molecular electronic structure is one in which the wavefunction is described by a *molecular orbital*. A spatial orbital, $\psi_i\left(\vec{r}\right)$, describes the distribution of an electron at position $\vec{r}$ so that the probability of finding that electron in a region $d\vec{r}$ is equal to 1. The addition of spin takes the *spatial orbital* to a *spin orbital*, i.e. for one electron

$$\chi\left(\vec{x}\right) = \begin{cases} \psi\left(\vec{r}\right)\alpha(s) \\ \psi\left(\vec{r}\right)\beta(s) \end{cases}. \tag{2.1.9}$$

To put everything into perspective, we can write, for an N - electron system, the fully anti-symmetrized determinant wavefunction that minimizes the total energy of the fully interacting Hamiltonian (2.1.2) as

$$\Psi_{HF}\left(\vec{x}_1, \vec{x}_2, ..., \vec{x}_N\right) = \left(N!\right)^{-1/2} \begin{vmatrix} \chi_i\left(\vec{x}_1\right) & \chi_j\left(\vec{x}_1\right) & \cdots & \chi_k\left(\vec{x}_1\right) \\ \chi_i\left(\vec{x}_2\right) & \chi_j\left(\vec{x}_2\right) & \cdots & \chi_k\left(\vec{x}_2\right) \\ \vdots & \vdots & & \vdots \\ \chi_i\left(\vec{x}_N\right) & \chi_j\left(\vec{x}_N\right) & \cdots & \chi_k\left(\vec{x}_N\right) \end{vmatrix}, \tag{2.1.10}$$

where $\left(N!\right)^{-1/2}$ is the normalization constant. This matrix and its solution are the *Slater Determinant*, and the entire procedure, the *Hartree-Fock* Approximation (HF).

Antisymmetrizing a Hartree product and obtaining a Slater determinant gives rise to what is called the *exchange* effect. This is due to the requirement that $\left|\Psi^2\right|$ be invariant under the exchange between space and spin coordinates of two electrons. The Slater determinant thereby incorporates *exchange-correlation*, but, only between electrons with similar spin.[7] The energy expectation value for this wavefunction is found through

$$\mathrm{E}_{HF} = \left\langle \Psi_{HF} \left| \hat{\mathrm{H}} \right| \Psi_{HF} \right\rangle = \sum_{i=1}^{N} H_i + \frac{1}{2} \sum_{i,j=1}^{N} \left(J_{ij} - K_{ij} \right) \tag{2.1.11}$$

with the *Coulomb Integral*, J_{ij}, and the exchange integral, K_{ij} defined as (See [7]):

$$H_i = \int \psi_i^* \left(\vec{r}\right) \left[-\frac{1}{2}\nabla^2 + v\left(\vec{r}\right) \right] \psi_i \left(\vec{r}\right) d\vec{r} \tag{2.1.12}$$

$$J_{ij} = \iint \psi_i \left(\vec{r}_1\right) \psi_i^* \left(\vec{r}_1\right) \frac{1}{r_{12}} \psi_j^* \left(\vec{r}_2\right) \psi_j \left(\vec{r}_2\right) d\vec{r}_1 d\vec{r}_2 \tag{2.1.13}$$

$$K_{ij} = \iint \psi_i^* \left(\vec{r}_1\right) \psi_j \left(\vec{r}_1\right) \frac{1}{r_{12}} \psi_i \left(\vec{r}_2\right) \psi_j^* \left(\vec{r}_2\right) d\vec{r}_1 d\vec{r}_2 . \tag{2.1.14}$$

Again, the ground state of the orbitals is determined through the variational principle applied to this expression while keeping the orbitals orthogonal and normalized. This then produces the *Hartree-Fock,* or rather, what is now known as, the *SCF Equations*[10]

$$\left[-\frac{1}{2}\nabla^2 + v_{ext}\left(\vec{r}\right) + \int \frac{\rho\left(\vec{r}'\right)}{\left|\vec{r}-\vec{r}'\right|} d\vec{r}' \right] \psi_i\left(\vec{r}\right) + \int v_X\left(\vec{r},\vec{r}'\right) \psi_i\left(\vec{r}'\right) d\vec{r}' = \varepsilon_i \psi_i\left(\vec{r}\right) \tag{2.1.15}$$

where v_X describes the non-local exchange potential, i.e.

$$\int v_X\left(\vec{r},\vec{r}'\right) \psi_i\left(\vec{r}'\right) d\vec{r}' = -\sum_{j}^{N} \int \frac{\psi_j\left(\vec{r}\right) \psi_j^*\left(\vec{r}\right)}{\left|\vec{r}-\vec{r}'\right|} \psi_i\left(\vec{r}'\right) d\vec{r}', \tag{2.1.16}$$

and

14

$$\rho\left(\vec{r}_1\right) = N\int\cdots\int\left|\Psi\left(\vec{x}_1, \vec{x}_2, \ldots, \vec{x}_N\right)\right|^2 ds_1 d\vec{x}_2 \cdots d\vec{x}_N \qquad (2.1.17)$$

the number of electrons per unit volume within a certain, given, state, where upon integration,

yields the total number of electrons[8,9], i.e.

$$\int \rho\left(\vec{r}\right) d\vec{r} = N . \qquad (2.1.18)$$

The Hartree-Fock equations give us the underlying detail of non-interacting electrons within the

influence of a *mean-field potential*. This potential is comprised of both the potential of the

Coulomb repulsion and potential from the non-local exchange interaction. These Hartree-Fock

equations are fully capable of incorporating antisymmetry through inclusion of the exchange

contribution term (2.1.16), which prevents the electron from interaction with itself. Should this

happen, the Coulomb repulsion potential term will in turn equate to zero, e.g. when $i = j$.

The exact wavefunction cannot be described by one or any "simple" combination of

determinants, as such this only adds to the list of discrepancies within the Hartree-Fock

approach. Due to this inadequacy, the variational principle brings forth a difference between the

actual ground state energy and the ground state energy obtained within the HF procedure. This

difference is called the correlation energy. Correlation energy is a product of the inaccuracy in

the determination of the proper repulsion of the electrons with one another. The repulsion

experienced by any electron is merely an average density of the remaining electrons, rather than

explicitly. Attempts to correct this energy difference have led to the extension of (2.1.10)

through the addition of more Slater determinants, a linear combination of atomic orbitals

(LCAO), known as Configuration Interaction (CI). Each of these atomic orbitals fitted with an

appropriate normalization constant, to wit, the collection of these constants is termed the basis.

But, in actuality the determination of an exact ground state wavefunction for a particular system

involves hundreds and even <u>thousands</u> of these basis set constants, and for each orbital in

question. There is an extension to this formalism called Full Configuration Interaction (FCI), that attempts to represent the orbitals in the same manner as the total system wavefunction, by replacing each basis set coefficient with its own wavefunction. In either scheme, CI or FCI, one would need an infinite number of basis terms to arrive at the exact system wavefunction. This is, of course, computationally impossible, thus CI and FCI even for more than a few atoms and electrons becomes very expensive, very early.

2.2 Density Functional Theory

It is at this point which electronic structure calculation diverges into two camps. The first being the further improvements made to CI and FCI over the years to form new methods based on them. And, the second, an alternative calculation method based solely on replacing the multi-electron wavefunction and its Schrödinger equation with the electron density $\rho\left(\vec{r}\right)$, (see 2.1.18). The latter has proven it to be a viable alternative to previous calculation methods, especially for large and complex systems. This versatility has added to its growth, both in popularity and efforts to extend it in complexity. This approach has been aptly named Density Functional Theory (DFT). DFT is one of the most successful quantum mechanical based calculations applied to matter to date, and not only to clusters of atoms, but also to the periodic systems of solids.[11]

Making the assumption that the electron density can describe the full electron wavefunction is not completely unfounded. The procedure was essentially done in reverse previously within the time-independent Schrödinger Equation (2.1.1) and its Hamiltonian (2.1.2), as we shall see below. The Hamiltonian is defined by the variables, N, number of electrons, Z,

nuclei, and the distance between them, $\vec{R}$. Using (2.1.18) we can immediately find the N. Also, it was E.B. Wilson, a theoretical spectroscopist, that proposed one year later after the two theorems of Hohenburg and Kohn[12], that the electron density can be used to determine both position and charges of the nuclei, Z. He did this based on the fact that the density reaches a maxima at the nuclei positions, using the equation

$$Z_\alpha = \frac{-1}{2\overline{\rho(0)}} \left[\frac{\partial \overline{\rho}(r_\alpha)}{\partial r_\alpha} \right]_{r_\alpha = 0} , \qquad (2.2.1)$$

where $\overline{\rho}(\vec{r})$ is termed the spherical average of ρ.[8,9] The fact that one can derive the necessary variables required for the Hamiltonian simply using the density is useful, as the density can be observed experimentally.

DFT today as we know it today began with those theorems of Hohenburg and Kohn. The first of which declares that *the external potential* $v(\vec{r})$ *is determined, within a trivial additive constant, by the electron density*. This tells us also that the wavefunction can be determined from the density along with all the other properties of the system. The second theorem incorporates the variational principle for wavefunctions. Stating,

For a trial density $\widetilde{\rho}(\vec{r}) \geq 0$ *and* $\int \widetilde{\rho}(\vec{r}) d\vec{r} = N$,

$$E_0 \leq E_v\left[\widetilde{\rho}\right], \qquad (2.2.2)$$

where $E_v\left[\widetilde{\rho}\right]$ *is the energy functional of,*

$$E_v\left[\widetilde{\rho}\right] = \mathrm{T}[\rho] + U_{ne}[\rho] + V_{ee}[\rho] = \int \rho(\vec{r}) v(\vec{r}) d\vec{r} + F_{HK}[\rho] \qquad (2.2.3)$$

with

$$F_{HK}[\rho] = F[\rho] = \mathrm{T}[\rho] + V_{ee}[\rho]. \qquad (2.2.4)$$

Where $T[\rho]$ is the kinetic energy term, $V_{ee}[\rho]$ the Coulomb repulsion, and $U_{ne}[\rho]$ the nuclei-electron interaction. Together, the kinetic energy and Coulomb repulsion sum to become the Hohenburg-Kohn functional (2.2.4), $F_{HK}[\rho]$. Thus, assuming that $E_\nu[\tilde{\rho}]$ is differentiable, the two theorems yield the fundamental expression of DFT[9],

$$\delta\left[E[\rho] - \mu\left(\int \rho(\vec{r})d\vec{r} - N\right)\right] = 0, \qquad (2.2.5)$$

(with μ the electronic chemical potential) which tells us that the ground-state energy and its density are the minimum to some functional $E[\rho]$. This entire procedure has shown us that there exists what can be considered a *universal* functional, $E[\rho]$, and if known can be inserted into (2.2.5). But, since the exact form of the Hohenburg-Kohn functional is not something we are privy to, the two theorems do not establish a method or routine in which to solve the Schrödinger equation; rather show that the electron density is a principle key in linking the physical system to quantum mechanical calculation. There are many implementations of DFT, and performing the variational principle continuously to find the ground-state wavefunction of a system is not the most efficient. It was not until the work of Kohn-Sham that a modern day DFT procedure unfolds.

To summarize, Kohn and Sham proposed a method in which to incorporate a non-interacting system from single-electron orbitals such that the kinetic energy can be computed to relatively good precision separately from the electron-electron repulsion term.[14] This procedure allows the calculation of the majority of the systems properties fairly precisely, whilst leaving a very small percentage of those properties to be calculated by another functional. The above can be seen below, in (2.2.7), where we rewrite (2.2.3) to produce this desired separation, and rewrite the Coulomb repulsion and interaction in terms of the density, known as the Hartree energy

$$V_H[\rho] = \frac{1}{2} \int \frac{\rho(\vec{r}_1)\rho(\vec{r}_2)}{|\vec{r}_1 - \vec{r}_2|} d\vec{r}_1 d\vec{r}_2 . \qquad (2.2.6)$$

Combining everything together to obtain

$$E[\rho] = T_s[\rho] + U_{ext}[\rho] + V_H[\rho] + E_{xc}[\rho], \qquad (2.2.7)$$

and with the relation

$$T[\rho] = T_S[\rho] + T_C[\rho], \qquad (2.2.8)$$

the S subscript for single-particle, C for correlation. T_S is not known precisely in terms of the density, ρ, but can be written in terms of the single-particle orbitals $\phi_i(\vec{r})$ of a non-interacting system:

$$T_S[\rho] = -\frac{1}{2} \sum_i^N \langle \phi_i | \nabla^2 | \phi_i \rangle \qquad (2.2.9)$$

and within this system both kinetic energy and density are known from the orbitals and yields the true ground-state density of

$$\rho(\vec{r}) = \sum_i^N |\phi_i|^2 . \qquad (2.2.10)$$

$E_{xc}[\rho]$, the exchange-correlation energy, is written as

$$E_{xc}[\rho] = (T[\rho] - T_S[\rho]) + (V_{ee}[\rho] - V_H[\rho]), \qquad (2.2.11)$$

and is merely the addition of all the error that arises when using a non-interacting system for the kinetic energy and in treating the electron-electron repulsion and interaction classically. Applying the variational principle the orbitals satisfy the equations of

$$\left[-\frac{1}{2}\nabla^2 + v_{ext}(\vec{r}) + \int \frac{\rho(\vec{r})}{|\vec{r} - \vec{r}'|} d\vec{r}' + v_{xc}(\vec{r}) \right] \phi_i(\vec{r}) = \varepsilon_i \phi_i(\vec{r}), \qquad (2.2.12)$$

19

where $v_{xc}(\vec{r})$ represents a local multiplicative potential, a functional derivative of $E_{xc}[\rho]$ with respect to the density, or

$$v_{xc}(\vec{r}) = \frac{\delta E_{xc}[\rho]}{\delta \rho}. \qquad (2.2.13)$$

Equations (2.2.12) and (2.2.13) represent the Kohn-Sham Equations, and since their publication there have been numerous attempts to approximate and further eliminate the unknowns within the exchange-correlation functional, and represents a growing field of research.[13]

Today, there are a wide variety of exchange-correlation functionals that one can choose from. But, the first of these was the Local Density Approximation, LDA. LDA was based on the methodology that the system in question could be studied through the use of a uniform electron gas, to which a near exact result could be obtained, as the density was a constant obtained by division of N by V (the volume of gas). Thus, if the electron-electron interaction is approximated by the Hartree potential, the total energy can be easily computed. Under this calculation scheme, the Kohn-Sham equations can be solved for exactly. The LDA exchange-correlation expression is written as

$$E_{xc}^{LDA}[\rho] = \int \rho(\vec{r}) \varepsilon_{xc}\left[\rho(\vec{r})\right] d\vec{r}, \qquad (2.2.14)$$

where $\varepsilon_{xc}(\rho)$ is taken to be the exchange-correlation energy of the electron gas, and can be separated into exchange and correlation parts as

$$\varepsilon_{xc}(\rho) = \varepsilon_x(\rho) + \varepsilon_c(\rho). \qquad (2.2.15)$$

The separation of the energy allows for an additional freedom in representing the density. This *unrestricted* form allows for the consideration of the contributions of spin-up and spin-down

electrons independently. This unrestricted form paves the way for LSDA, local-spin density approximation, which is written similarly to (2.2.14) as

$$E_{xc}^{LSDA}\left[\rho_\uparrow, \rho_\downarrow\right] = \int \rho\left(\vec{r}\right)\varepsilon_{xc}\left[\rho_\uparrow\left(\vec{r}\right), \rho_\downarrow\left(\vec{r}\right)\right]d\vec{r}. \tag{2.2.16}$$

For many decades LDA and LSDA have been used in calculating band structures and total energies in physics when applied to solid-state systems. In quantum chemistry, both functionals have fallen into disfavor, because of the failure to provide accurate results needed when discussing characteristics of bonding and reactivity. These results include correct structure prediction, but also tend to overestimate the binding energy. The problem with LDA and LSDA is that they only incorporate very localized values for the electron density. In physical systems, and any system of interest, the electron density is not a constant, thus contributing further to this inaccuracy. What followed in the years to come was the development of the Generalized Gradient Approximation (GGA). GGA includes and incorporates the gradient of the electron density, $\nabla\rho\left(\vec{r}\right)$. This extends equation (2.2.14) again into the following form,

$$E_{xc}^{GGA}\left[\rho_\uparrow, \rho\downarrow\right] = \int \rho\left(\vec{r}\right)\varepsilon_{xc}\left[\rho_\uparrow\left(\vec{r}\right), \rho_\downarrow\left(\vec{r}\right), \nabla\rho_\uparrow\left(\vec{r}\right), \nabla\rho_\downarrow\left(\vec{r}\right)\right]d\vec{r}. \tag{2.2.17}$$

This exchange-correlation technique is the most widely used in DFT today and stands as the starting point for some of the more complicated exchange-correlation functionals available.

Once the selection of an exchange-correlation functional has been decided upon, we can apply the Kohn-Sham equations and iteratively solve the Schrödinger equation. These iterations, the self-consistent procedure are performed in the following way: first, suppose a set of atomic orbitals, $\{\Omega_i\}_{in}$, then construct a trail wavefunction and density. Lastly, solve the Schrödinger equation and obtain a new set of orbitals, $\{\Omega_i\}_{out}$ and corresponding density. This list of steps is

continued until $\{\Omega_i\}_{in} \cong \{\Omega_i\}_{out}$, at which time the resultant energy and density are considered to be at the ground-state for a particular system.

2.3 Theoretical Methods

The tools that employed DFT in our investigation of ligand-protected clusters were the Amsterdam Density Functional codes employing a linear combination of Slater-type orbitals in expressing the Kohn-Sham atomic orbitals.[15] These orbitals, say ϕ, are used in turn used to construct the wavefunction, i.e.

$$\Psi_i(\vec{r}) = \sum_\mu c_{\mu i} \phi_\mu(\vec{r}), \tag{2.2.18}$$

where $c_{\mu i}$ represents the orbital coefficient with index i. The results presented herein were computed using the exchange-correlation functional of Perdew-Burke-Ernzerhof (PBE)[16,17]. The PBE functional can be broken into two parts, exchange and correlation. The exchange, with enhancement factor, F_x, can be written

$$F_x(s) = 1 + \kappa - \frac{\kappa}{\left(1 + \frac{\mu s^2}{\kappa}\right)}, \tag{2.2.19}$$

where κ, μ are predefined constants, and s, the dimensionless reduced gradient of order m (where for PBE: m=1) written as

$$s_m = \frac{\left|\nabla^m \rho(\vec{r})\right|}{2^m (3\pi^2)^{\frac{m}{3}} (\rho(\vec{r}))^{\left(1 + \frac{m}{3}\right)}}. \tag{2.2.20}$$

Thus, the first gradient is written,

$$s_1 \equiv s = \frac{\left|\nabla \vec{r}_s\right|}{2\left(\frac{2\pi}{3}\right)^{1/3} \vec{r}_s} , \qquad (2.2.21)$$

with $\vec{r}_s \equiv r_s\left(\vec{r}\right)$, the normalized average distance between electrons. Secondly, the correlation (without corrective term *H*) is defined as

$$E_c^{GGA-PBE}\left[\rho_\uparrow\left(\vec{r}\right), \rho_\downarrow\left(\vec{r}\right)\right] = \int \rho\left(\vec{r}\right)\left\{\varepsilon_c\left(\vec{r}_s, \zeta\right)\right\}d\vec{r} , \qquad (2.2.22)$$

where $\zeta\left(\vec{r}\right)$ is the spin-polarization term

$$\zeta\left(\vec{r}\right) = \frac{\left(\rho_\uparrow\left(\vec{r}\right) - \rho_\downarrow\left(\vec{r}\right)\right)}{\rho\left(\vec{r}\right)} . \qquad (2.2.23)$$

The basis set used in our calculations under the STO configuration where of Triple-Zeta Double Valence Polarized (TZ2P), where this scheme of "multiple-zeta" valence functions is done to calculate the same valence orbital with three basis functions in order to increase flexibility of the calculation. The term "polarized" denotes the use of additive terms to the basis to include contributions of orbitals with higher angular momentum. This is done to account for the non-spherical geometry of the atom, and its orbit clouds.[17] We go further in the calculations as to fix the inner most electron orbitals close to the atoms using what is termed a Frozen-Core basis set. Fixing the inner most electrons, especially within heavier atoms, decreases the total number of basis functions needed and reduces the computing time required. This slight-of-hand is fully accounted for when using the Zeroth Order Regular Approximation (ZORA).[19-23] ZORA accounts for all electrons within the basis set and incorporates spin-orbit coupling, as well as relativistic effects.

# Chapter 3. The $Ag_4Ni_2(DMSA)_4$ Cluster: Results

3.1 $Ag_4Ni_2(DMSA)_4$ & Isomer

Firstly, we describe our findings as a result of the theoretical investigation into the electronic structure of the $Ag_4Ni_2(DMSA)_4$ cluster. The beginning of this inquiry involved numerous configurations of Ag and Ni atoms bonding directly or indirectly through the sulfur atoms. Furthermore, the DMSA ligands were configured also in a multitude of placements. In every case, the geometry found through this construction of atoms was relaxed, until the forces between one another reached a minimum threshold. In consideration of any possible magnetic configurations, the procedure was repeated, but beginning the relaxation process with a predefined magnetization.

The lowest energy structure is shown below in Figure 5(A) (isomer 1), while the geometry of Figure 5(B) (isomer 2) is the first isomer upwards in energy by 0.61 electron-volts to that of 1. In either case, these two geometries both exhibit a distorted octahedral with respect to the four silver and two nickel atoms, with sulfur at the Ag—Ni vertices.[24] Also, it can be seen that there are eight Ag—S and eight Ni—S bonds within both structures.[6]
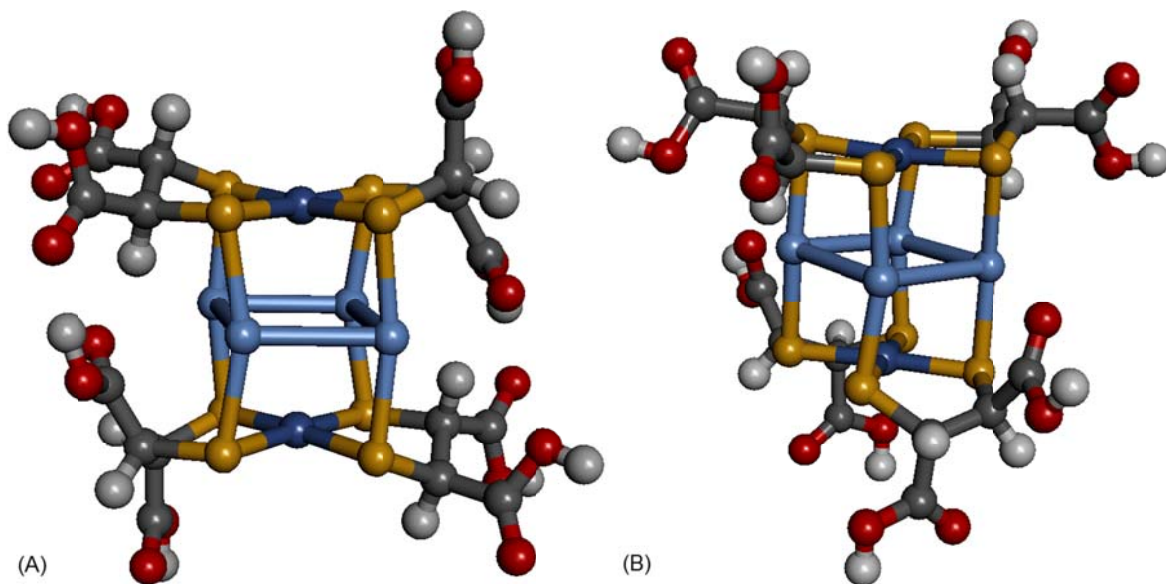
Figure 5. (A) Ground state structure of $Ag_4Ni_2(DMSA)_4$ as found through DFT (isomer 1). (B) First ground state isomer higher in energy. (isomer 2).

Simply by inspection, we can also see that $Ni(DMSA)_2$ plays an integral role within them, in relatively the same manner regardless of DMSA orientation. Calculations of solitary $Ni(DMSA)_2$ (Figure 6) has shown that the ground state geometry has a square-planar motif with sulfur atoms around nickel, with splitting of the 3d orbital on Ni resulting in triplet multiplicity of the complex. This triplet multiplicity will prove to be critical, as we shall see below.
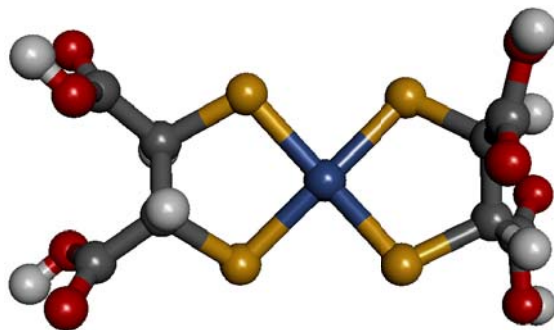

Figure 6. The $Ni(DMSA)_2$ complex.

The binding energy of Ni and one DMSA ligand is 4.58 electron-volts, and the second DMSA, 3.28 electron-volts. Both binding energies are in stark contrast to the binding energy for DMSA to Ag, of 2.01 electron-volts.

3.2 Absorption Spectra

To further determine the correct structure of the cluster, additional UV-Vis spectra were simulated. The optical spectrum of Figure 3B is within reasonable agreement with these simulations. The first calculated excitement is that of 590 nm which is consistent with the weak absorption experimentally observed at 600 nm. The results of these simulations have shown that isomer 2 has a strong absorbance at 452 nm, which was not consistent with experiment, and subsequently led to the belief that isomer 1 was the most dominant. A third isomer (Figure 7) was also theoretically calculated which showed to be 0.82 eV higher in energy to that of isomer 1, where the nickel atoms were adjacent to one another, and has a strong absorption at 700 nm. The simulated UV-Vis spectrum for all three isomers is plotted within Figure 8.
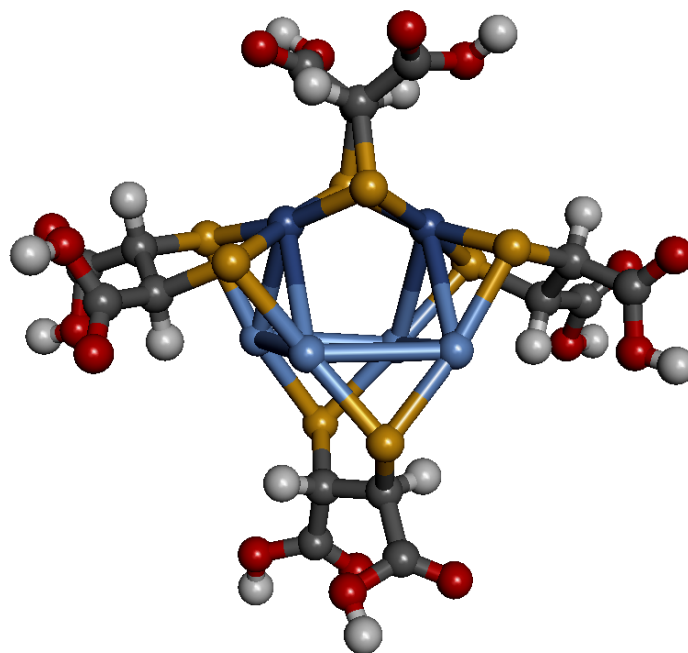
Figure 7. Third isomer of $Ag_4Ni_2(DMSA)_4$ with adjacent nickel atoms.
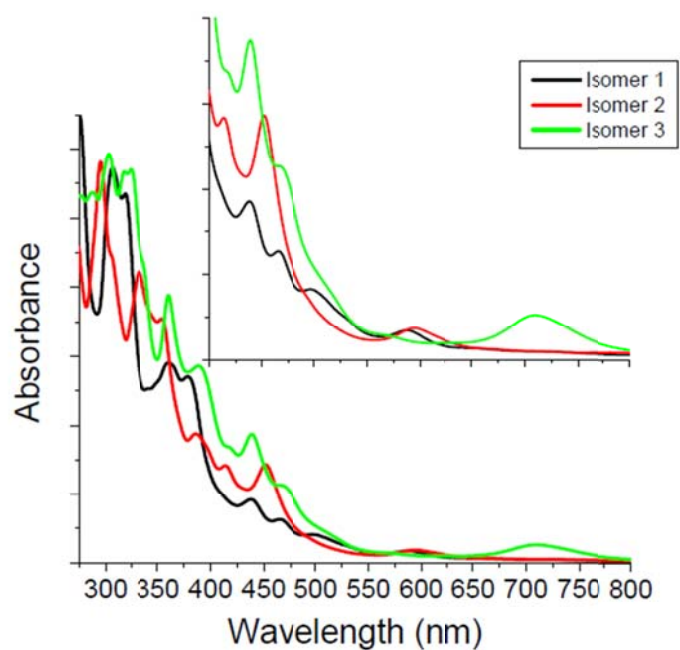
Figure 8. Simulated UV-Vis absorption spectra for the two isomers of Figure 5 in addition to the third of Figure 7. Inset shows a magnification of the region 400-800 nm.

3.3 Origin of Stability

As outlined above in section 3.1, stability begins with the larger binding energy of the Ni to DMSA than Ag. From above we know the ground state of $Ni(DMSA)_2$ is of triplet multiplicity, thus deficient of two electrons and contains an open electronic shell. The total cluster stability arises from this need to fill the outer shell. As such, the two $Ni(DMSA)_2$ complexes present in all isomers, are in need of four silver atoms. The Ag atoms thereby donate their charge to Ni, thus as a result of a large transfer of charge, yields a bimetallic core. This process can then be viewed and confirmed through their respective density-of-states (DOS), where the HOMO-LUMO (Highest Occupied Molecular Orbital, and Lowest Unoccupied Molecular Orbital) gap of isomer 1 is 1.28 eV (Figure 9) and 1.40 eV for isomer 2.
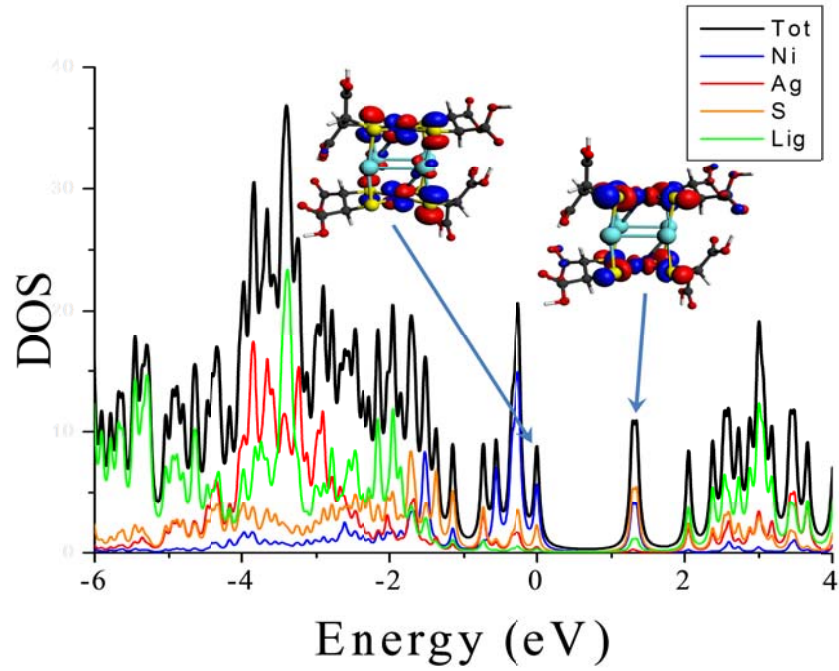
Figure 9. Density Of States (DOS) for the $Ag_4Ni_2(DMSA)_4$ of isomer 1 (Figure 5A). The isosurfaces for both HOMO and LUMO states are also shown. (Reproduced from [24])

Chapter 4. Fragment Characterization

One technique to probe the structure of a cluster is through the use of fragmentation experiments. While X-ray crystallography allows for the determination of a cluster's geometry, making crystals that are pure enough such that their geometry can be revealed is often impossible. Mass spectrometry identifies the stoichiometry of the cluster, but does not offer any information pertaining to the structure. MS/MS experiments where a cluster is isolated in the gas phase and ionized through electrospray is a powerful tool for revealing their structure. In this chapter we use theoretical methods to improve further upon MS/MS to further understand the fragmentation pattern of the $Ag_4Ni_2(DMSA)_4$ cluster.

Starting with an example cluster, say A_xB_y we can devise numerous pathways for the separation of the two atoms A and B, all which are governed by

$$\Delta E + A_xB_y = A_{x-n}B_{y-m} + A_nB_m . \qquad (4.1.1)$$

where ΔE represents the energy required to cluster into pieces. The pathways in which ΔE is small are preferred, strictly on the basis of energetics. Therefore, a cluster will preferentially break into its most stable fragments. As a consequence of this, the first step towards determining and understanding fragmentation patterns involves the search for the binding energies for various fragments. A second criterion for identifying stable fragments is the electron affinity (E.A.), which represents the energy required to remove an electron from a cluster. A cluster A^- will thus have an electron affinity that can be calculated using (4.1.2), below.

$$E.A. = E\left[A\right] - E\left[A^-\right] \qquad\qquad (4.1.2)$$

The E.A. for charged clusters provides information with regards to which cluster fragment will be more likely to keep the charge and is an important criterion because mass spectrometry only detects charged species. A third quantity which proves useful is the energy difference between the HOMO and LUMO states. Clusters with a large energy difference, or "gap", are resistant towards either donating or receiving electronic charge. Thus, these clusters can be considered as stable or inert.

Given the above, we begin with the calculation and presentation of all possible cluster fragment constituents. Starting with $Ag_n^{0/-}$ clusters and their geometries, this is then followed by $Ag_nS_m^{0/-}$ (n = 1 – 7, m = 0 – 4). We then move forward to bimetallic $Ag_nNi_m^{0/-}$ (n = 1 – 7, m = 1 – 2). All leading toward discussions of the $Ag_4Ni_2(DMSA)_4$ cluster core identification, and finally the total cluster fragmentation energetics.

4.1 The Structure & Energetics of $Ag_nS_m^{w}$ (n = 1 – 7, m = 0 – 4, w = 0, -1)

To understand the fragmentation pattern, we first investigate the HOMO-LUMO gap and energetic stability of $Ag_nS_m^{0/-}$ clusters. From here we would like to fully understand the bonding between the silver and sulfur atoms. The first of these calculations begins with the determination of the pure silver clusters which can be seen below in Figure 10 for clusters of two to seven atoms in size. Additionally, Figure 11 displays the ground state geometries of various combinations of silver and sulfur, silver ranging from one to seven.
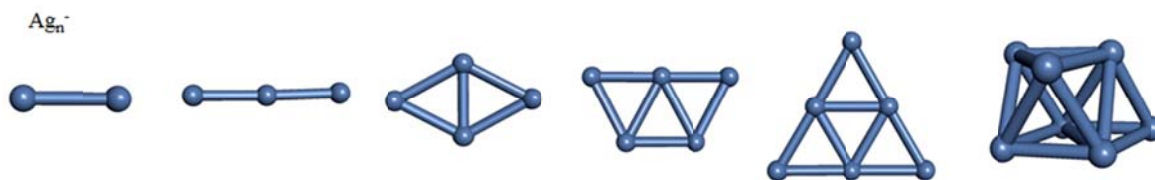
Figure 10. Ground state geometries as calculated for pure silver clusters Ag_n^- (n = 2 – 7).

The ground state of silver anionic clusters is not new, but obtaining their energies using the formalism outlined above is necessary.

In continuing the ground state search, full structure and electronic calculations for the various combinations of $Ag_nS_m^w$, where (n = 1 – 7, m = 0 – 4, w = 0, -1), were completed. These geometries can be seen in Figure 11, and we can immediately observe that the addition of sulfur drives the ground state geometries of the silver clusters from a planar arrangement into a three dimensional one earlier in its series. The HOMO-LUMO gaps for these combinations of silver and sulfur are displayed below in Figure 12, with key interest being paid on the silver clusters of the $Ag_nS_3^-$, and Ag_nS_4 series'.
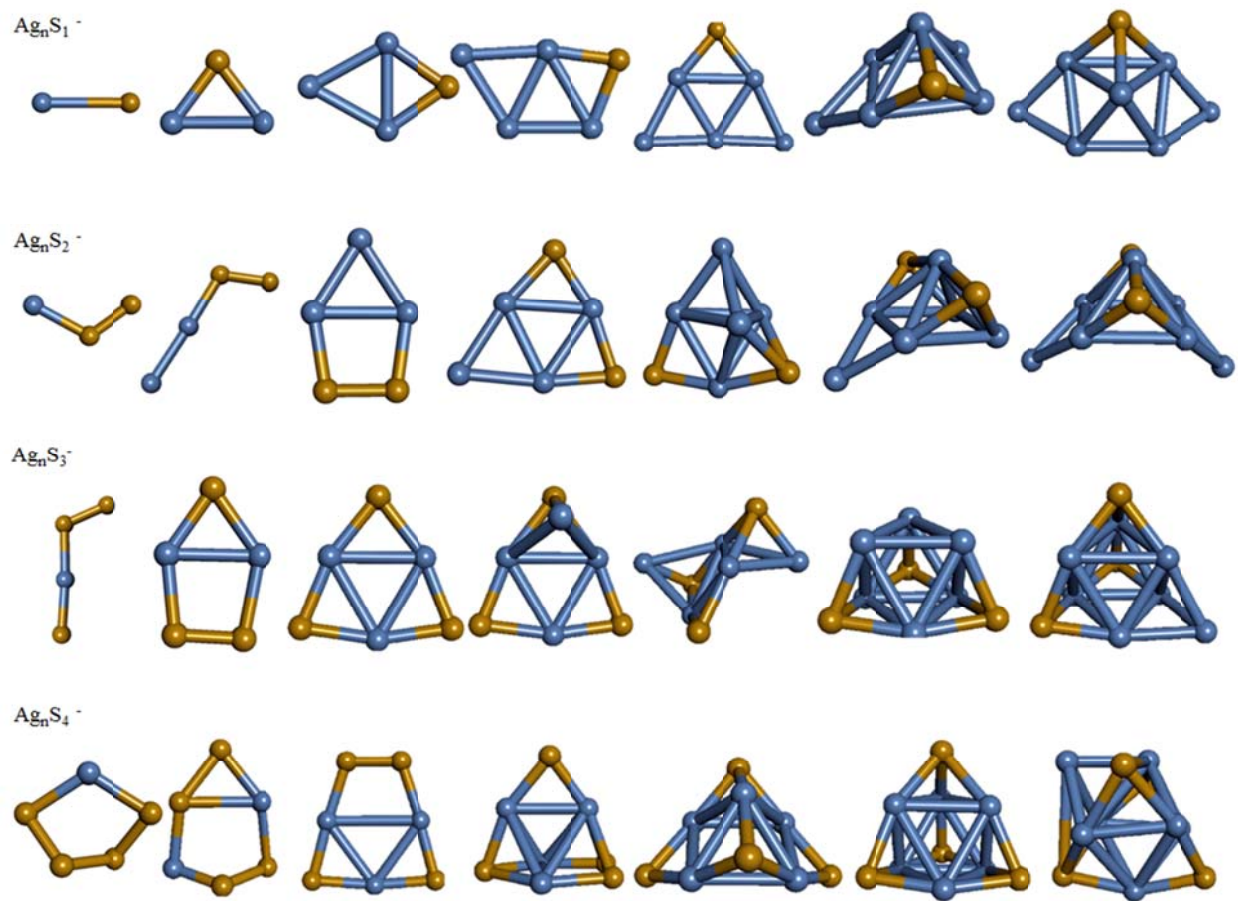
Figure 11. Ground state geometries for $Ag_nS_m^-$ (n = 1 – 7, m = 1 – 4). (Ag increasing L-R).
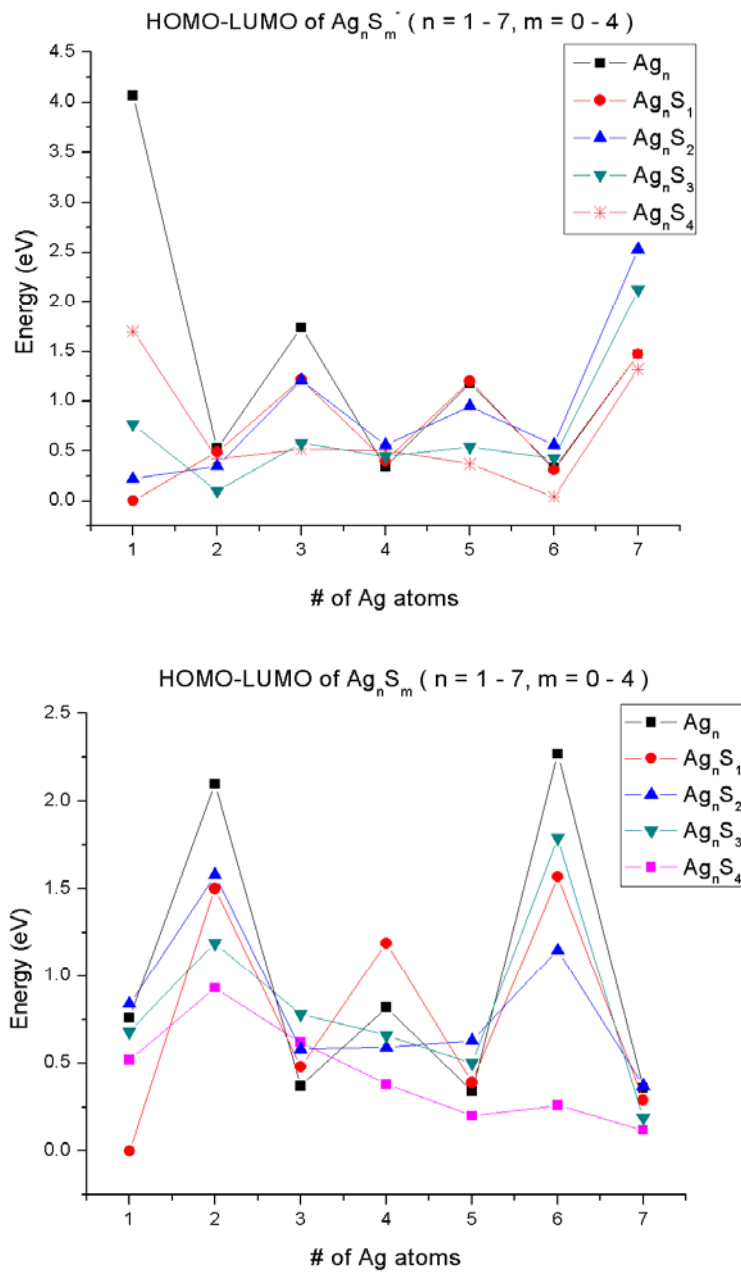
Figure 12. Energy graphs showing the HOMO-LUMO gaps for several combinations of Ag and S clusters of anion (top) and neutral (bottom) varieties.

Within both graphs of Figure 12 is it clear to see that there is a trend forming as the addition of sulfur tends to reduce the HOMO-LUMO gap of the pure Ag_n^- clusters at all sizes except those of n=5, and 7. For n=7 it is the only cluster with a drastic increase in HOMO-LUMO gap. In the neutral graph, only Ag_4S has a larger HOMO-LUMO gap than the pure silver cluster with the same number of silver atoms. In this analysis, we only consider clusters with even electrons as the odd numbered ones tend to have smaller and indistinguishable HOMO-LUMO gaps that do not indicate their relative stability. Next, we focus on the two sets of clusters, the Ag_6S_m, and $Ag_7S_m^-$. The progression of HOMO-LUMO gap for both clusters can be viewed in Figures 16 and 17, respectively.

To further analyze the stability of the Ag_nS_m clusters we now examine the graphs of silver removal energy in Figure 13. As sulfur atoms are added to Ag_6, the Ag removal increases, after an initial drop for Ag_6S_m. This implies that the Ag_6S clusters are becoming more stable through the addition of sulfur. Thus, as the gap increases, the total stability increases. Next, the examination of the silver removal energies within the $Ag_7S_m^-$ clusters in Figure 13 (bottom). The addition of sulfur to the Ag_7^- clusters gradually increases the silver removal energy from 1.3 eV in pure Ag_7^- to 2.25 eV for $Ag_7S_4^-$. This again implies the addition of sulfur is increasing the stability. This increase is consistent with the increase in HOMO-LUMO gap through the addition of sulfur within Figure 12. A general trend in the addition of sulfurs seems to increase the silver removal energy within nearly all Ag_nS_m clusters. This not only tells us that adding sulfur to silver decreases the HOMO-LUMO gap, but also increases the energetic stability of the cluster. An indication that the sulfur binding energy is increasing as the size of the silver cluster grows.

Further criteria used to understand the effect of sulfurization on the stability of silver clusters is the sulfur removal energy, seen in the graphs of Figure 14. The sulfur removal energies are consistently larger than those of silver, due to the fact of the covalent bonding between silver and sulfur is much stronger than the metallic bonding between silver atoms. Figure 14 also shows the sulfur removal energy increasing with size, especially for the Ag_nS^- series. For the case of $Ag_7S_m^-$, the sulfur removal energy is increasing with the size; this indicates that the cluster is becoming more stable through the addition of sulfur, although less so for the $Ag_7S_4^-$. The exception to this trend is that of $Ag_5S_m^-$, where the first sulfur binds most strongly than subsequent additions. This trend is also apparent of the neutral clusters, also of Figure 13. In Ag_6S_m the binding energy for the first, second, and third sulfur combinations are successfully larger, but drops for the Ag_6S_4 cluster. This indicates that while the HOMO-LUMO gap of Ag_6S_m cluster is decreasing, the energetic stability is increasing.

The final criterion in the assessment of the stability of the $Ag_nS_m^{0/-}$ clusters is the electronic affinity, shown in Figure 15. The electronic affinity increases steadily with the addition of sulfur atoms. Sulfur is more electronegative than silver, which inherently stabilizes the anions, with Ag_6S_4, and $Ag_7S_4^-$ having large electron affinities of approximately 4 eV, and 3.8 eV, respectively. This seems to imply that either the anion, $Ag_7S_m^-$, is electronically stable, or the neutral, Ag_6S_4 is electronically unstable. This informs us that within a fragmentation experiment, the fragments of sulfur will keep the excess electron much more readily than the fragments of less sulfur, which makes the observation of sulfurized fragment species much more likely. We can also see minute evidence of the shell structure of the silver clusters; with eight valence electrons of Ag_7^- having a large electron affinity relative to other sizes.
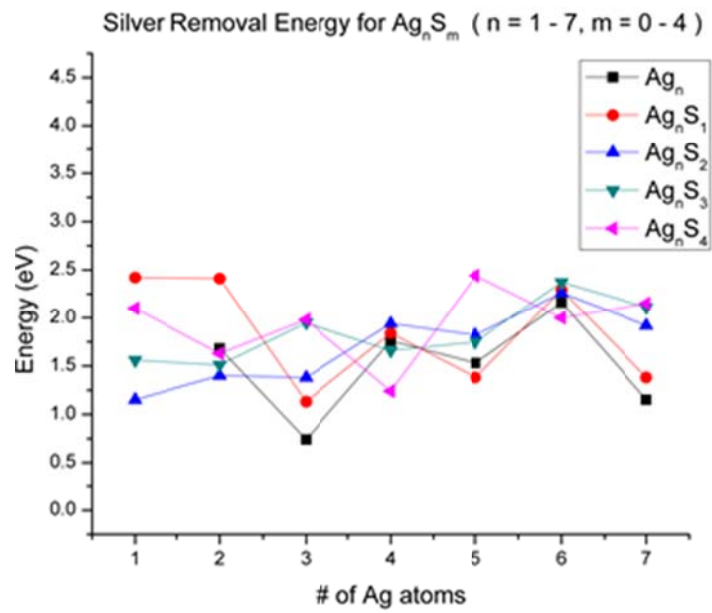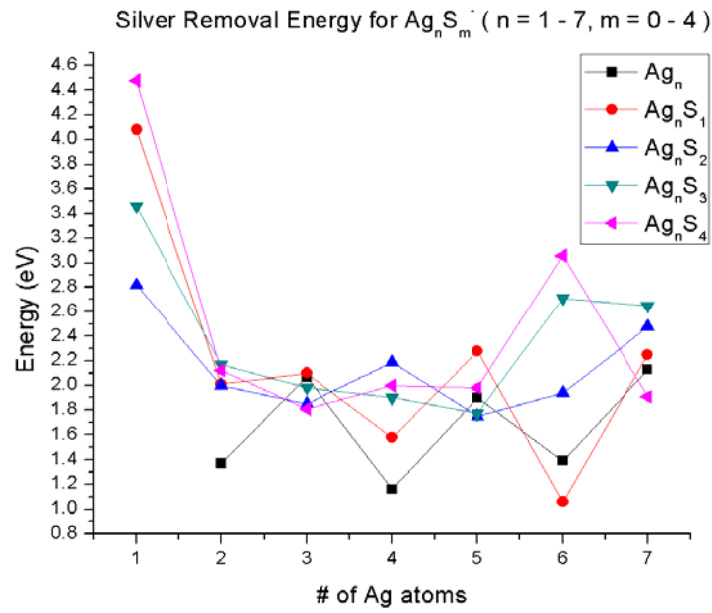
Figure 13. Energy required in removing silver from various combinations of Ag and S, both anionic (top) and neutral (bottom) varieties.

To summarize our results describe herein of the stability criteria, we have found the Ag_6S_m clusters are becoming energetically more stable with the addition of more sulfur, but are decreasing in electronic stability with the addition of silver. To gain insight into this contradiction, we turn to the electronic structure of the clusters presented in Figure 16, which displays the density of states for the Ag_6S_m cluster series, the projected density of states, and the Overlap Population Density of States (OPDOS) between the sulfur and silver orbitals of the cluster. Figure 16 shows that Ag_6 has a planar structure and large HOMO-LUMO gap of approximately 2.4 eV. This gap size is explained by the structure of the cluster itself, which has an electronic structure of the delocalized Ag 5s states of $|1S^2|\,|1P^4||1P^2|$, where the capital letters indicate a jellium-like delocalized orbital whose character is analogous to the aforementioned orbital.

The addition of sulfur within Ag_6S breaks the planar structure of the pure Ag_6 cluster, and pulls an unoccupied antibonding orbital downward to become the LUMO of the cluster. OPDOS is a tool used to understand the nature of bonding between two element species, where a positive OPDOS indicates constructive interference, and covalent bonding; and negative, destructive, which implies an antibonding orbital between the two species. The negative OPDOS of the LUMO, in conjunction with the LUMO isosurface (Figure 16), shows the antibonding state has lowered the HOMO-LUMO gap. This antibonding state is unoccupied, so whilst the gap has decreased, the energetic stability has risen. The addition of more sulfur has introduced new sets of antibonding orbitals, which keep the HOMO-LUMO gap lower than that of the pure Ag_6 cluster. The cluster of Ag_6S_4 is of special interest due to the fact that the cluster has taken on a distorted octahedral structure, whose ground state electronic structure contains two unpaired electrons. The four sulfur atoms within the cluster, each prefer to bond to three silver atoms,

38

which drives the structure towards this octahedral shape, but the cluster has six valence electrons, with eight needed for a closed shell. Thus, the energy is minimized within the cluster by moving to a triplet multiplicity with the electronic shell closed within the spin up channel. So we can say of the Ag_6S_4 cluster that the binding of sulfur first induces antibonding orbitals which form the LUMO of the cluster, which then reduces the HOMO-LUMO gap, and subsequently the binding of the sulfur drives the cluster to an octahedral geometry and results in the cluster obtaining a triplet ground state.

We go on now to examine the electronic structure of the $Ag_7S_m^-$ clusters. Pure Ag_7^- has a HOMO-LUMO gap of approximately 1.5 eV, and a capped octahedral geometry. The eight electrons of Ag_7^- lead one to believe that this cluster should have a closed electronic shell and a large gap with spherical geometry. Similar to the neutral case, the addition of sulfur adds a LUMO to the cluster, which is antibonding in nature and has no immediate effect on the HOMO-LUMO gap. It is not until the addition of the second sulfur atom that the gap increases up to approximately 2.4 eV, due to the silver core being driven to a more compact geometry. The cluster maintains this large HOMO-LUMO gap within the $Ag_7S_3^-$ cluster. The compact geometry that the silver cluster undergoes as more sulfur atoms are added explains why the Ag_7 clusters have larger HOMO-LUMO gaps, as the silver core has eight valence electrons and yields a closed shell.

These results show that the bonding of sulfur in the silver cluster does not appear to change the effective valence electron count of the cluster. However, they do affect the geometry, driving the planar silver cluster towards a more compact geometry. As in the case of Ag_6S_m, this "driving" force yielded the cluster into a triplet electronic state as the cluster became octahedral.
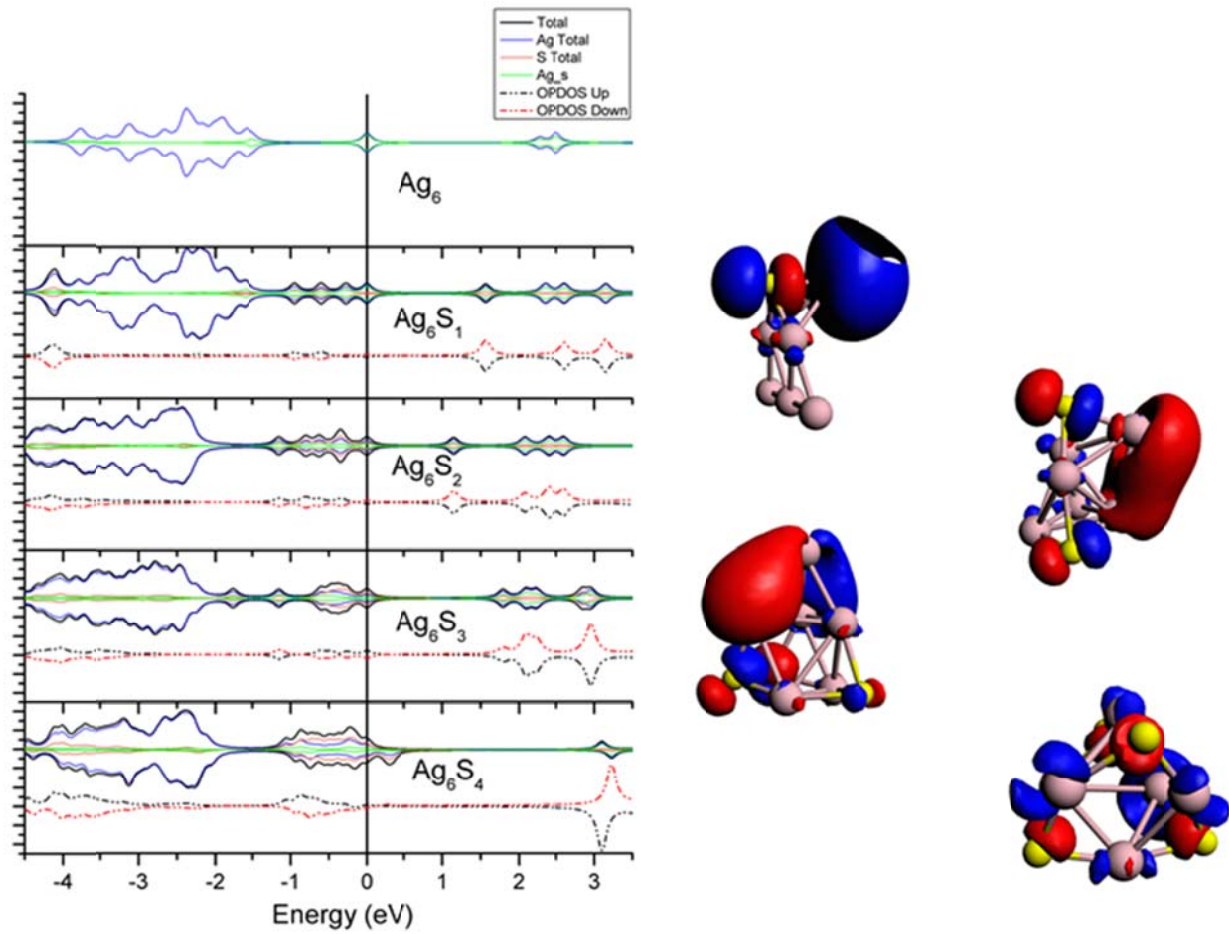
Whereas in the case of Ag_7S^-, the HOMO-LUMO gap was enhanced due to the compact

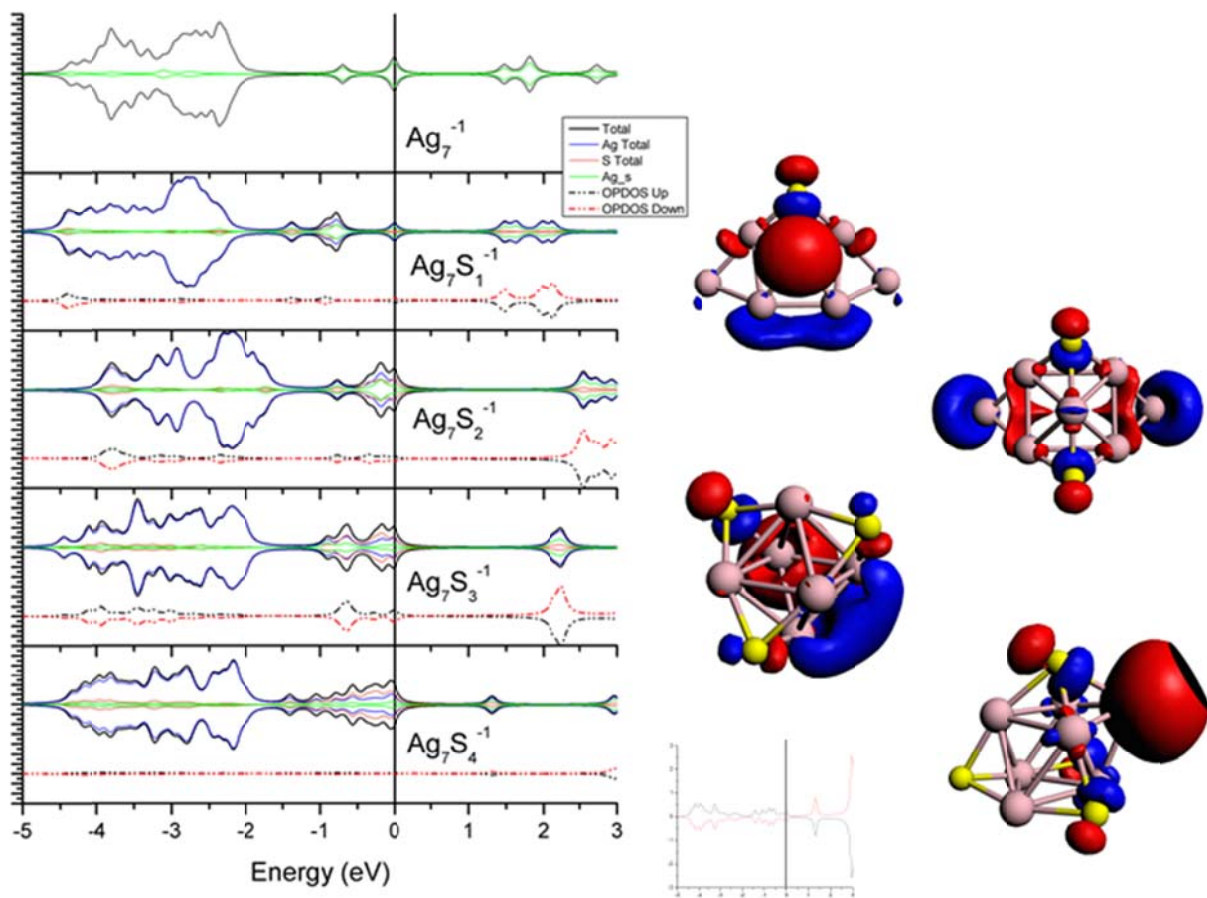geometry stabilizing the electronic structure of the silver core (Figure 17).
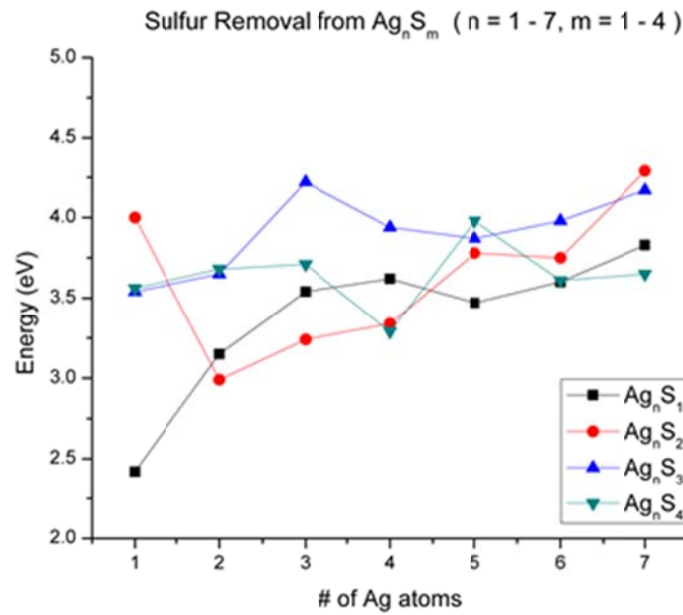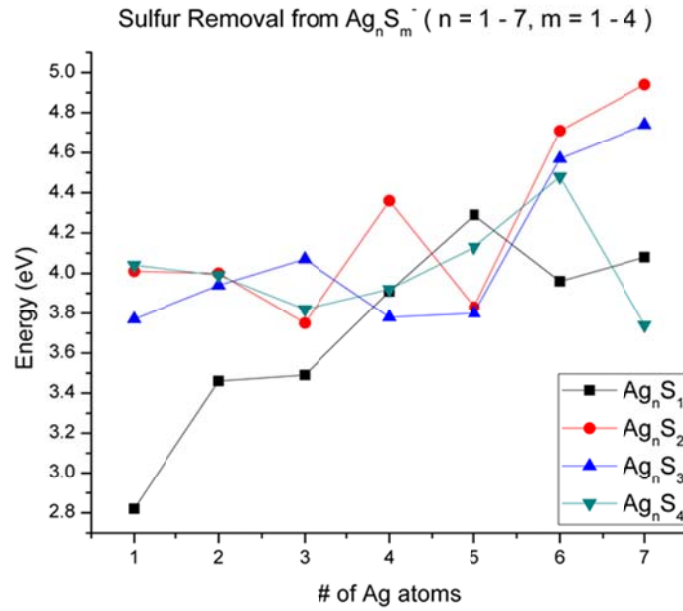
Figure 14. Energy required in removing sulfur from various combinations of Ag and S, both anionic (top) and neutral (bottom) varieties.
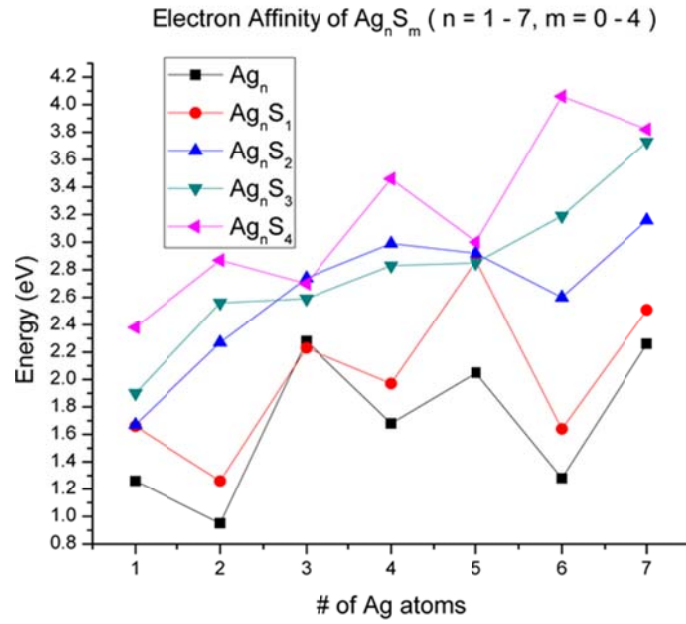
Figure 15. Electron affinity energies of Ag_nS_m (n = 1 – 7, m = 0 – 4)

Figure 16. HOMO-LUMO gap progression of Ag_6S_m (m = 0 – 4) with corresponding LUMO isosurface (right).

Figure 17. HOMO-LUMO gap progression of $Ag_7S_m^-$ (m =0 – 4) with corresponding LUMO isosurface. Inset shows adjusted OPDOS of $Ag_7S_4^-$ for clarity.

4.2 The Structure & Energetics of Ag_nNi_m (n = 1 – 7, m = 1 – 4 , w = 0, -1)

A similar story to that of the silver-sulfur clusters can be told for clusters of Ag and Ni, whose ground state geometries can be seen in Figure 18, where in Figure 19 (top) we see that HOMO-LUMO gap of anionic pure silver and silver-nickel clusters alternate with some regularity. The HOMO-LUMO gap of the bimetallic Ag_nNi_m clusters are much lower than that of pure silver clusters, due to the fact that nickel does not have the delocalized character of silver, which results in clusters with larger HOMO-LUMO gaps. It is not until the addition of a second nickel atom, the Ag_nNi_2, that this regularity changes pattern. Within this cluster series the HOMO-LUMO gap begins at an energy of approximately 0.5 eV, but as silver is added the gap size alternates less frequently and with smaller change in energy. This continues up to Ag_7Ni_2 where the gap is almost non-existent. Irregularity is also present within the neutral case of Figure 19 (bottom), with the difference between Ag_5Ni_2 and Ag_6Ni_2 is negligible, but the energy difference in HOMO-LUMO between clusters Ag_6Ni_2 and Ag_7Ni_2 increases dramatically.

We can progress from here and compare Figure 20 to Figure 13 and see that silver removal stays relatively within the same area in terms of energy required, in both cluster combinations of Ni and S, anionic and neutral. But, in comparing Figure's 21 and 13 (bottom) we see that nickel (21), in anionic or neutral clusters, is easier to remove from silver clusters than sulfur within Ag_nS_m (13). This energy difference is even larger when discussing nickel removal in both anionic and neutral clusters with that of sulfur removal in $Ag_nS_m^-$ (Figure 13, top). The removal of nickel can be predicted to be easier than that of sulfur due to the fact that nickel has a

closed outer s orbital ($3d^8 4s^2$), whereas sulfur forms strong covalent bonds through its outer $3p^4$

shell. Because of this, the fragments of greater importance of the bimetallic $Ag_4Ni_2(DMSA)_4$

cluster are more likely to possess sulfur. Thus, our next topic will be the clusters of Ni_nS_m.
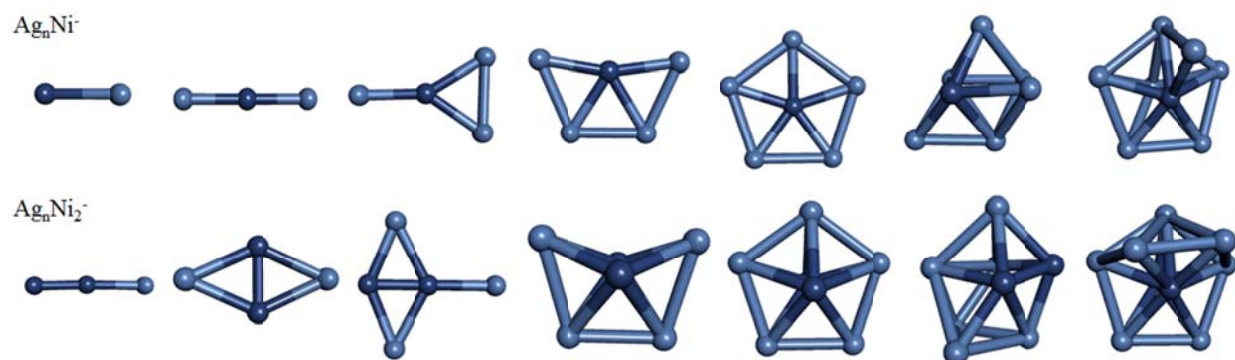
**Figure 18.** Ground state geometries for $Ag_nNi_m^-$ (n = 1 – 7, m = 1 – 2). (Ag increasing L-R)
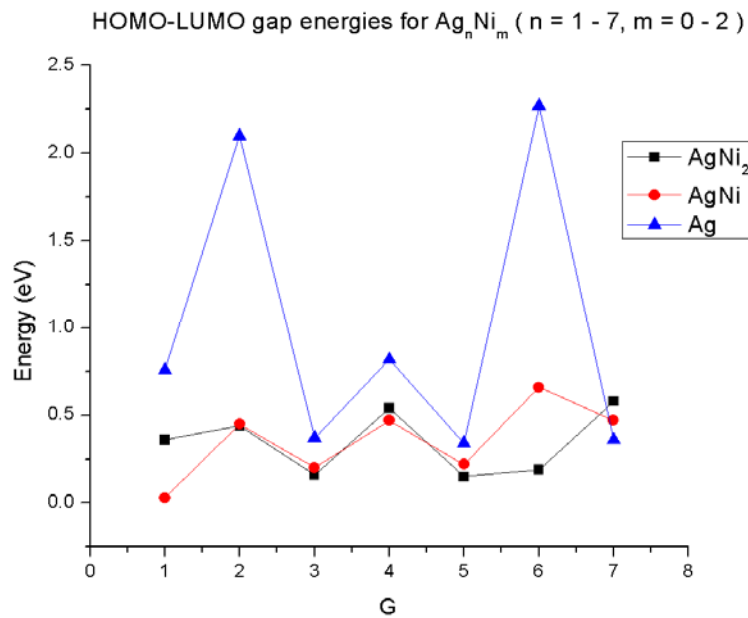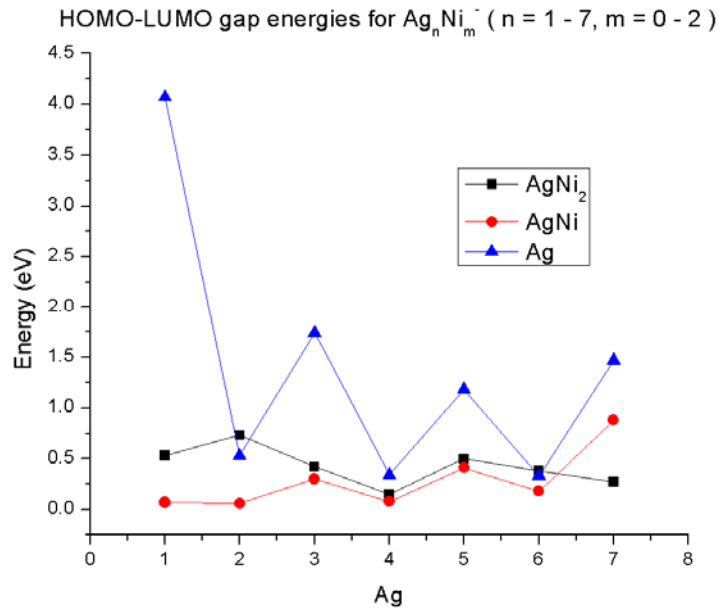
Figure 19. The HOMO-LUMO gap energies for several combinations of Ag and Ni, both anionic (top) and neutral (bottom) varieties.
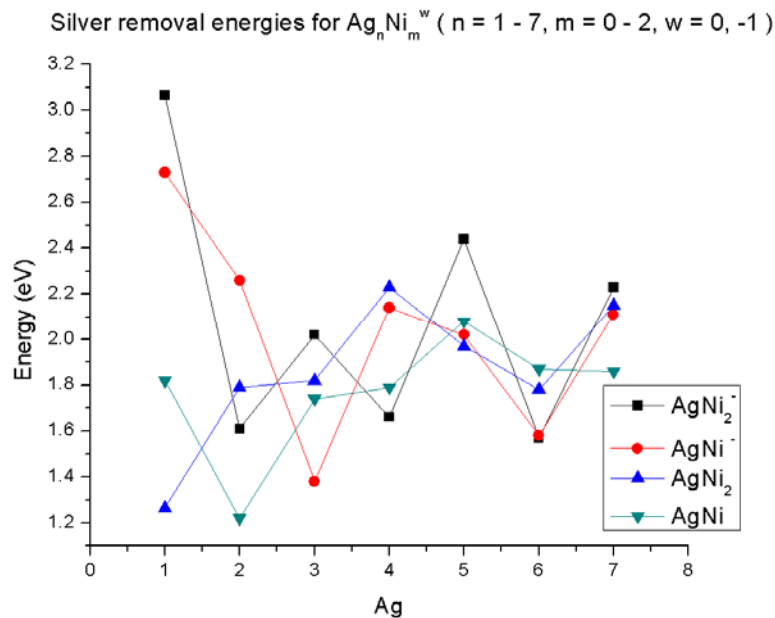
Figure 20. Graph showing the energy requirement for the removal of silver in various combinations of Ag and Ni, anionic and neutral.
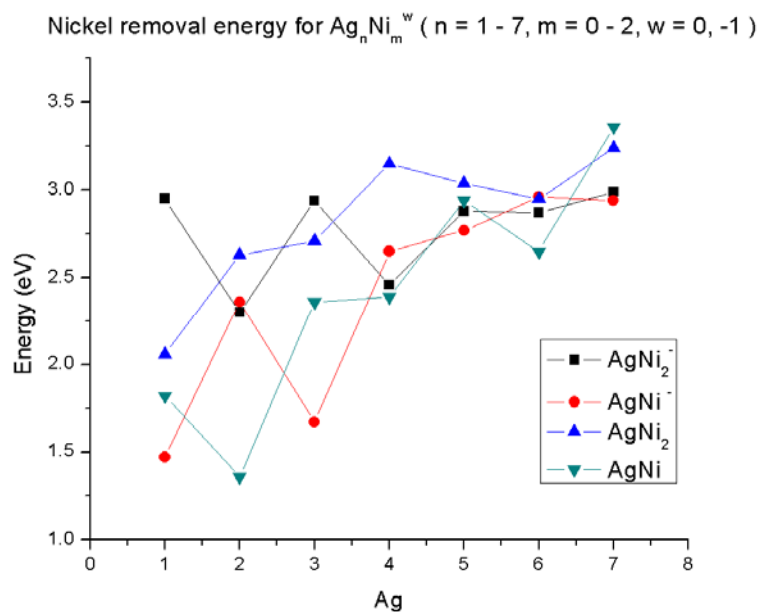
Figure 21. Graph showing the energy requirement for the removal of nickel in various combinations of Ag and Ni, anionic and neutral.
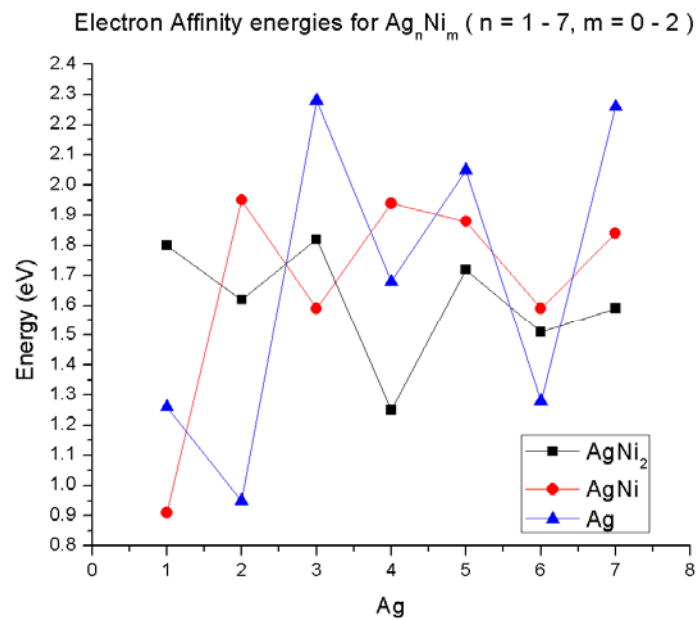
Figure 22. Electron affinity energies for various combinations of Ag and Ni.

4.3 The Structure & Energetics of $Ni_nS_m^w$ (n = 1 – 2, m = 1 – 4, w = 0, -1)

We finally arrive at critical part of the larger cluster characterization, the bonding between nickel and sulfur. This bonding is crucial to the stability of the cluster as a whole. We can see below in the removal of sulfur (Figure 23) and nickel (Figure 24) that our hypothesis of stabilization through Ni and S bonding is confirmed. This is most illustrated in the neutral combination of NiS_4 in Figure 23 with a sulfur removal energy just over 6 eV, and even more so for the combination of NiS_4^- in Figure 24, whose sulfur removal energy is now approximately 7.5 eV. This drastic energy difference is similar to the difference in energy of silver removal in Ag_1Ni_2 of Figure 20, and even more so to nickel removal in $AgNi^-$ of Figure 21.

In all series combinations, the sulfur removal energy of nickel clusters is much larger than the sulfur removal within those of silver clusters. But, through the eventual addition of silver these energies begin to stabilize until reaching near consensus at Ag_7. This implies that the fragmentation of the total bimetallic ligated cluster will be pushed towards fragments that will contain more nickel and sulfur. The ground-state geometries for $Ni_{1-2}S_{3-4}$ are displayed below in Figure 25.
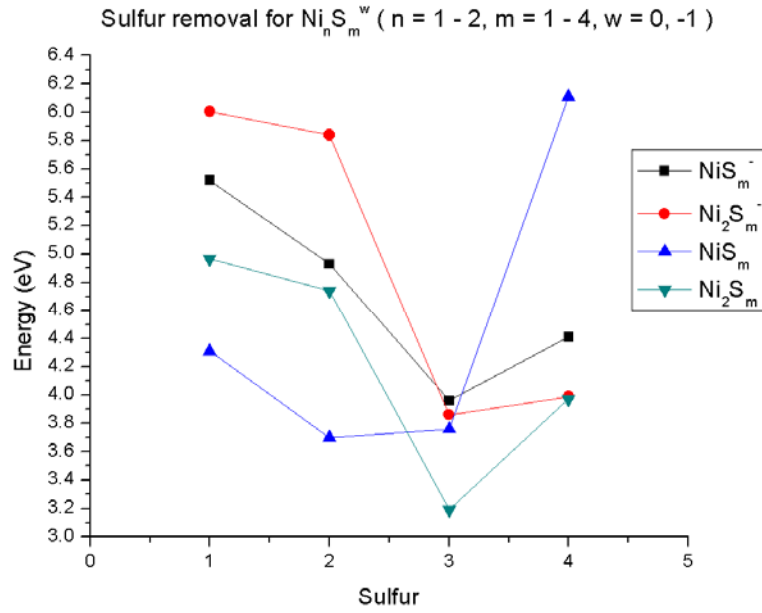
Figure 23. Graph showing the energy requirement for the removal of sulfur in various combinations of Ni and S, anionic and neutral.
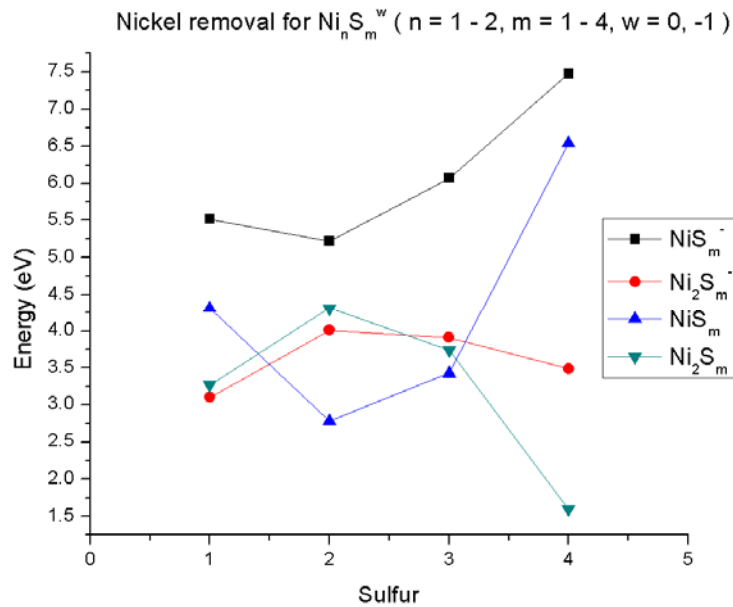
Figure 24. Graph showing the energy requirement for the removal of nickel in various combinations of Ni and S, anionic and neutral.
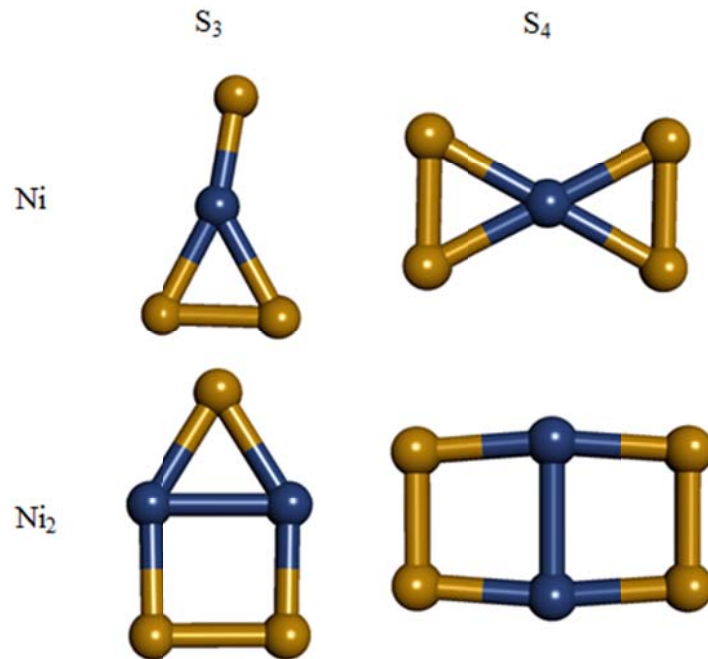
Figure 25. Ground state anionic cluster geometries for combinations of Ni_n (n = 1 – 2) and S_m (m = 3 – 4).
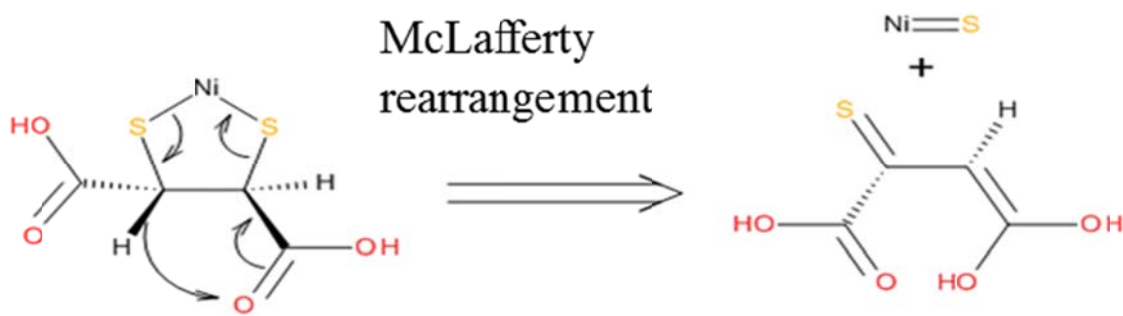
4.4 MS/MS Fragmentation

We next describe the experiment that fragments the ligand protected cluster. First, the cluster is put into the gas phase using electrospray, followed by mass spectrometry to identify the softly ionized species. The mass selected peak of 633 amu, which corresponds to $[Ni_2Ag_4(DMSA)_4-2H]^{2-}$ was then fragmented using electrospray mass spectrometry at various energies, 30 eV for the data of Figure 26. A procedure like this is conducted for two reasons; the first being to obtain full characterization of a cluster by analyzing all possible deformation mechanism and pathways. The second is less informational, but electrospray ionization and fragmentation can be used to create new, smaller clusters that vary widely in composition. In either case, MS/MS is the only way to discern what a cluster is composed of.

The first of these fragmentation experiments of the $Ag_4Ni_2(DMSA)_4$ cluster has yielded information in regards to both ligand removal and core geometry (Figure 26). It can be seen that the separation of core and ligand is a relatively common occurrence. Where the Ni(DMSA) ligand is a preferred fragment as yet another fragment has undergone a transformation similar to that of McLafferty rearrangement, using Ni(DMSA) as a precursor (Figure 27). This rearrangement cleaves an S—C bond, as well as one S—metal bond, and can be seen at the 146.8 amu mark, below. The ligand implies a core of formula $Ag_4Ni_2S_8$ and produces a core of $Ag_4Ni_2S_4$ which can be seen present at the 677.6 amu mark. The ligand produced as a result of the McLafferty rearrangement[25] (Figure 27) was studied extensively to derive the transition pathway in which this mechanism took place.

53
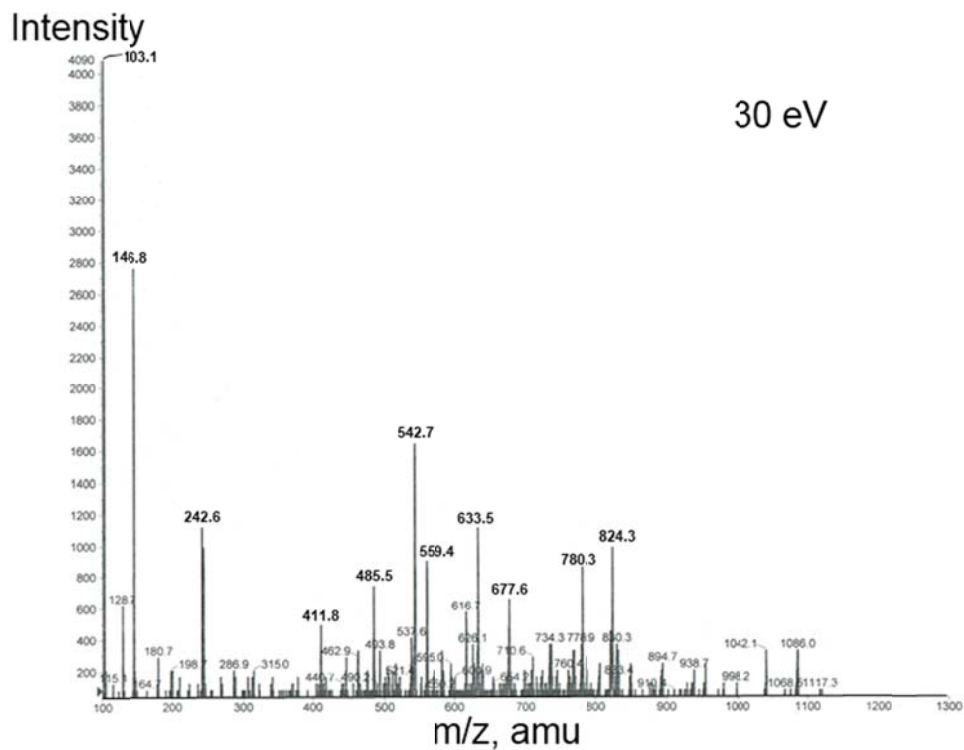
Figure 26. MS/MS of the $Ag_4Ni_2(DMSA)_4$ cluster through electrospray ionization MS at 30 eV. (MS/MS work done by collaborators in the A. Sen group at Pennsylvania State Univ.)

Figure 27. The McLafferty rearrangement mechanism of the Ni(DMSA) complex.

## 4.5 Ag$_4$Ni$_2$(DMSA)$_4$: Binding, Removal & Fragmentation Energetics

To understand the fragmentation patterns in the ligand protected cluster, we must examine the structure and energetics of the Ni$_x$Ag$_y$S$_z$ clusters. We begin with the neutral clusters, and even though these cannot be examined experimentally as MS/MS requires clusters that are charged, we use their geometry and corresponding energy to make inroads into the ones that we can. We can see in Figure 30 (top, bottom) the plots of removal energies required to fragment the Ni$_2$Ag$_n$S$_m$ (m = 3, 4) cluster down by an individual atom of Ni, Ag, S, or by complex of NiS. The data for the Ag$_n$Ni$_2$S$_4$ confirms that of the experimental in showing the Ag$_4$Ni$_2$S$_4$ cluster as the most stable, and requires the greatest amount of energy in removing an element. In the case of Ag$_n$Ni$_2$S$_3$, the neutral cluster also appears to have similar silver and sulfur removal energies for n = 1 – 4, indicating no strong size dependence on the stability. The stability of these clusters appears to be attributed to the additional number of sulfur atoms. The Figures of 28 and 29 above show some of the ground state geometries for anionic Ag$_n$, Ni$_m$, S$_3$ & S$_4$ combinations found in our study of the cluster fragments and can be considered the order in which silver atoms build upward to our final cluster.

Furthermore, to further understand the role of nickel within the larger cluster system, removal energies for various elements for clusters comprised of one nickel are computed. This procedure was completed for both anionic and neutral versions. The fruit of these labors can be visualized within Figures 31 and 33. We find for these clusters that solitary nickel and three sulfurs bind silver more weakly as compared to size. An example of this is exemplified in

55

Ag$_6$NiS$_3$, anionic and neutral. This also holds true for clusters of the formula Ag$_n$NiS$_4$, anionic and neutral. The electron affinity of the Ag$_x$Ni$_y$S$_z$ clusters are analyzed in Figures 34 and 35, and it is found that the energy is extremely large, especially for the Ag$_4$Ni$_2$S$_4$ cluster which has a halogen like affinity of approximately 3.7 eV. Indicating that in addition to the stability with respect to fragmentation, it also is unlikely to lose its excess electron.

The binding energy of nickel and sulfur in the Ag$_n$Ni$_2$S$_m$ clusters was consistently much larger than the removal energy for silver. This is consistent with the fragments revealing that the findings of Figure 36, in which the primary fragments, are Ag$_4$Ni$_2$S$_4$, from the variation on the McLafferty rearrangement, followed by the loss of a solitary silver atom to form Ag$_3$Ni$_2$S$_4$. Furthermore, the fragments identified are those of the Ag$_2$Ni$_2$S$_4$ and AgNiS$_4$ clusters. Higher energy fragmentation experiments reveal the presence of Ag$_n$Ni$_2$S$_3^-$ clusters, however the fragmentation pattern is consistent with the observed removal energies. This also reveals that within the fragmentation process, the core may be substantially rearranged, and this method which may allow for the gas phase synthesis of unusual size-selected cluster-assembled materials, using wet chemical synthesis methods to produce large quantities of specific clusters.
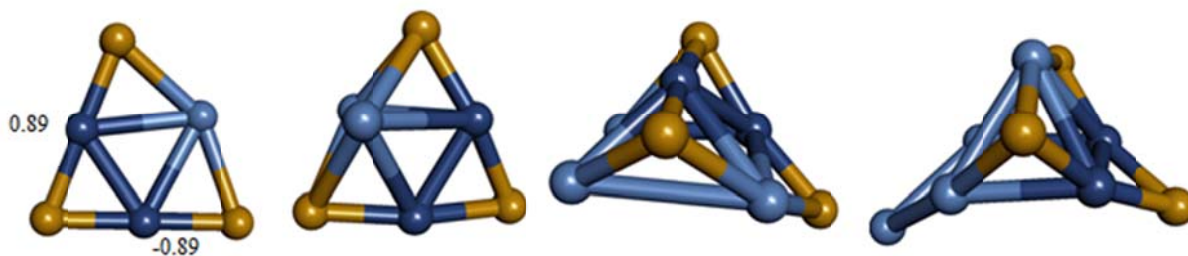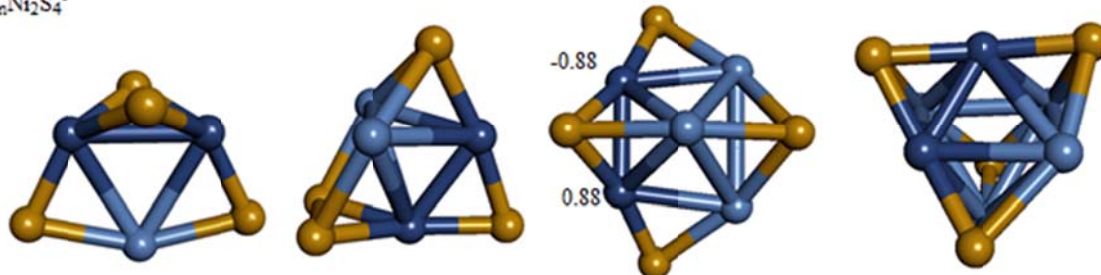
Ag$_n$NiS$_3$⁻
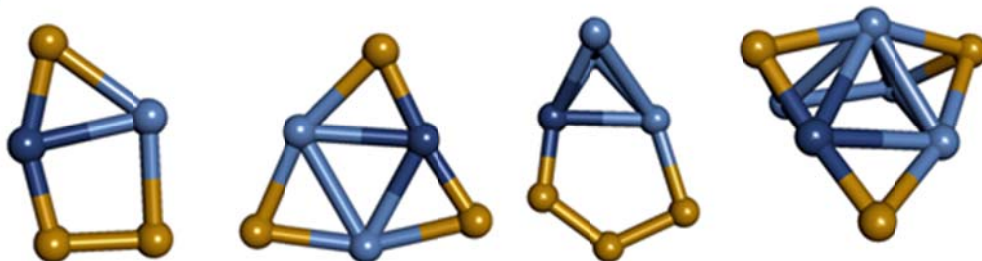
Ag$_n$NiS$_4$⁻
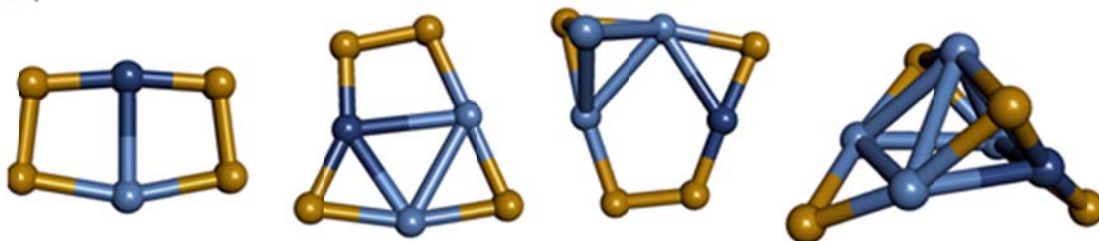
Figure 28. Combinations of Ag, Ni, and S$_3$ & S$_4$ anionic clusters. Number of silver atoms increasing from L-R.
(Clusters with numerical values assigned to nickel indicate direction and amount of charge (eV) as a result of anti-ferromagnetism.)

Ag$_n$Ni$_2$S$_3$⁻

0.89
-0.89

Ag$_n$Ni$_2$S$_4$⁻

-0.88
0.88

Figure 29. Combinations of Ag, Ni$_2$, and S$_3$ & S$_4$ anionic clusters. Number of silver atoms increasing from L-R.
(Clusters with numerical values assigned to nickel indicate direction and amount of charge (eV) as a result of anti-ferromagnetism.)
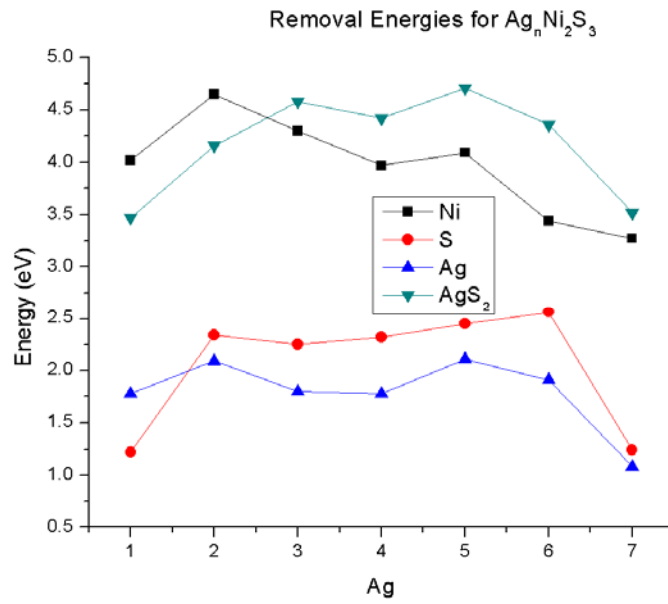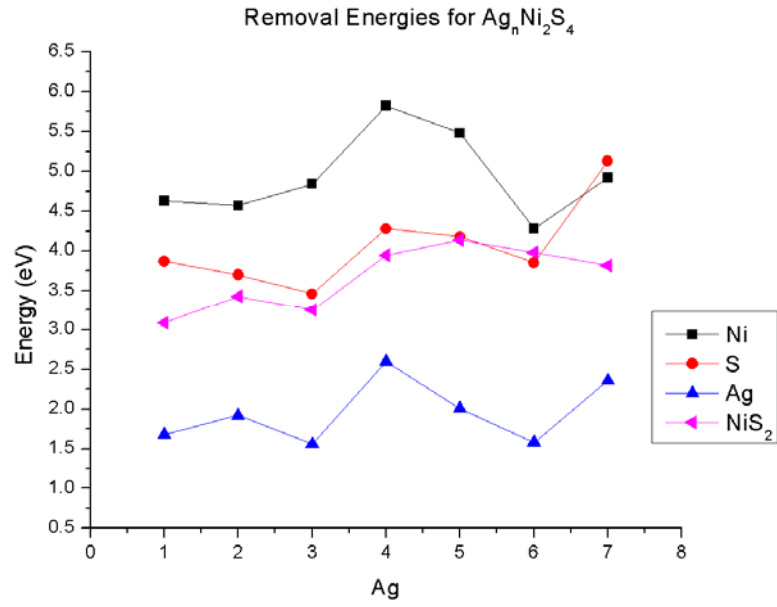
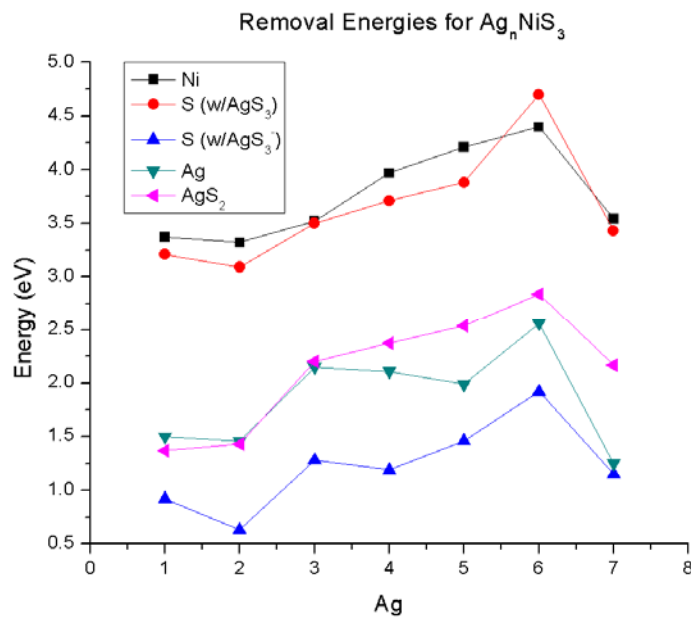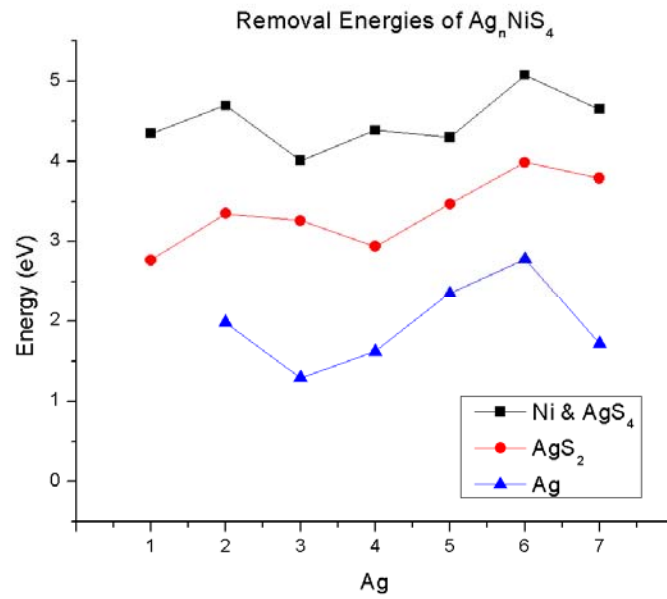**Figure 30.** Graphs showing the energy requirement for removal of various elements from $Ni_2Ag_nS_m$ ($m = 4$, top; $m = 3$, bottom).

Figure 31. Graphs showing the energy requirements for removal of various elements from $NiAg_nS_m$ (m = 4, top; m = 3, bottom).
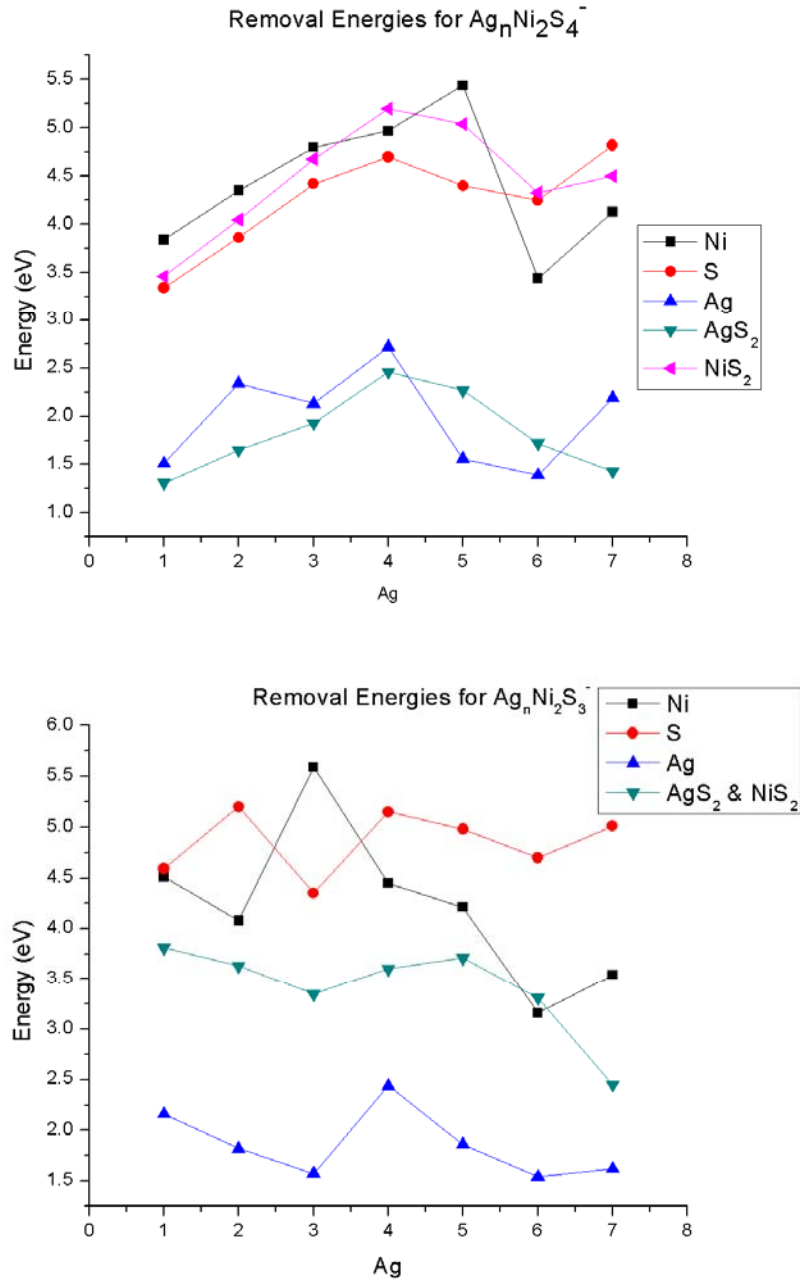
Figure 32. Graphs showing the energy requirements for removal of various elements from $Ni_2Ag_nS_m^-$ (m = 4, top; m = 3, bottom).
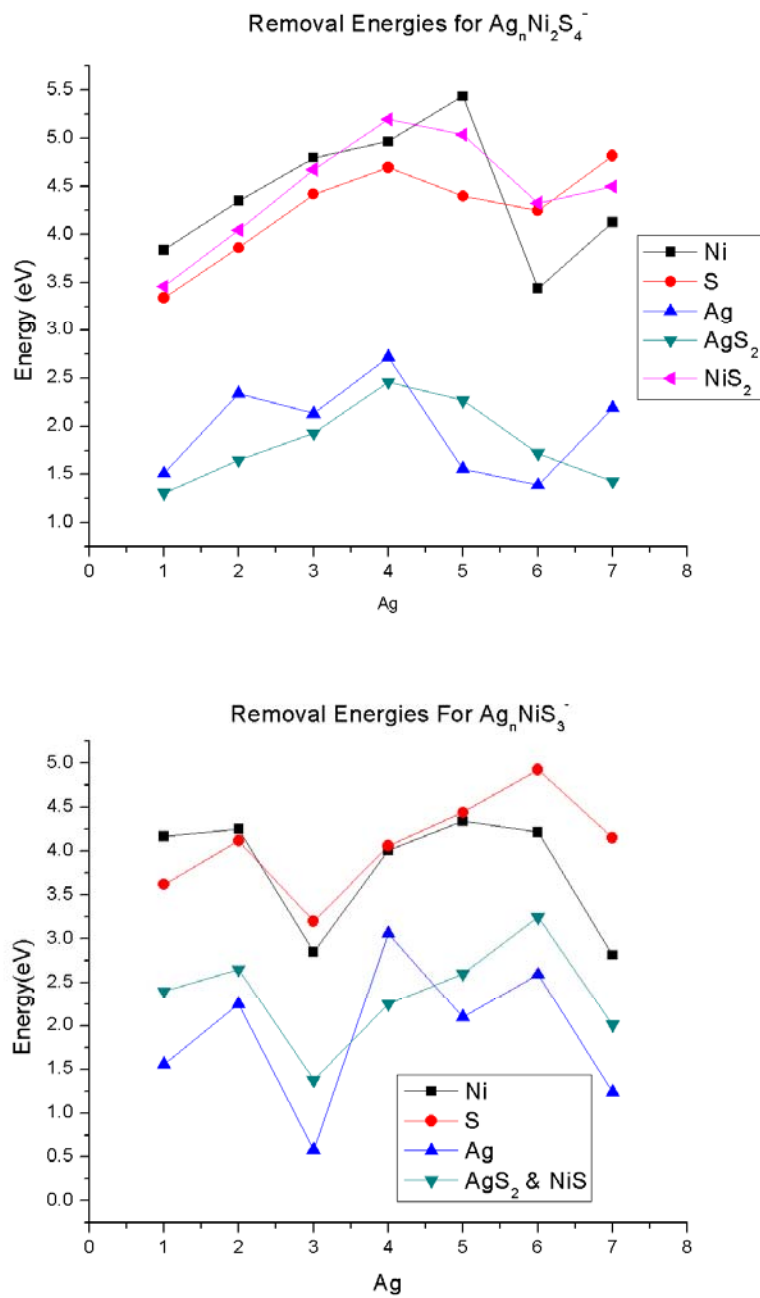
Figure 33. Graphs showing the energy requirements for the removal of various elements from $NiAg_nS_m^-$ (m = 4, top; m = 3, bottom).
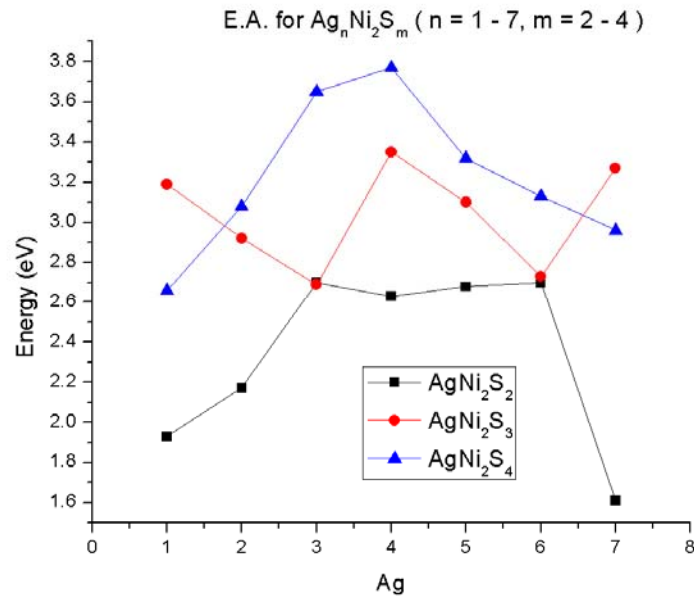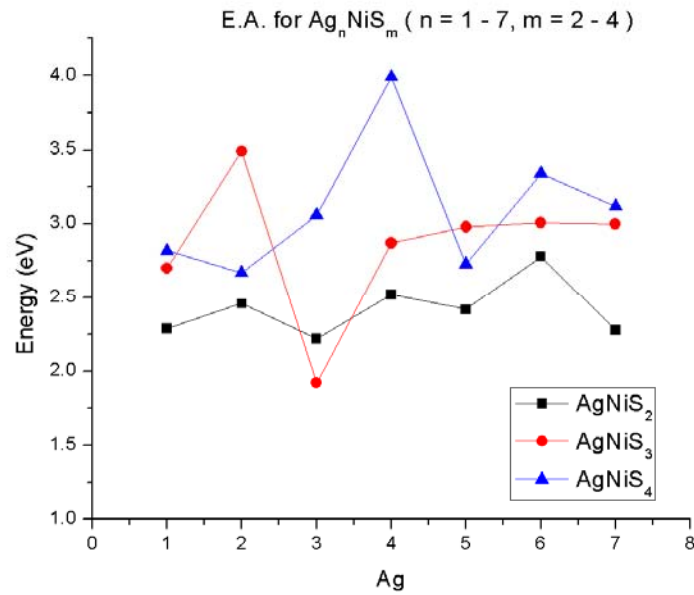
Figure 34. Electron Affinity graph for various combinations of $Ag_nNi_2S_m$ (m = 2 – 4).

Figure 35. Electron Affinity graph for various combinations of Ag_nNiS_m (m = 2 – 4).

The search for the correct core structure and atom placement goes further after the systematic calculation for the ground state of all the possible atom number combinations, placement, and charge was mounted. The ground state geometries led to the proper visualization and characterization of the major peaks within the fragmentation study not only at low energies, but also in higher energies, Figure 36. We can see below the assignment of these cluster geometries to their respective peaks, below.
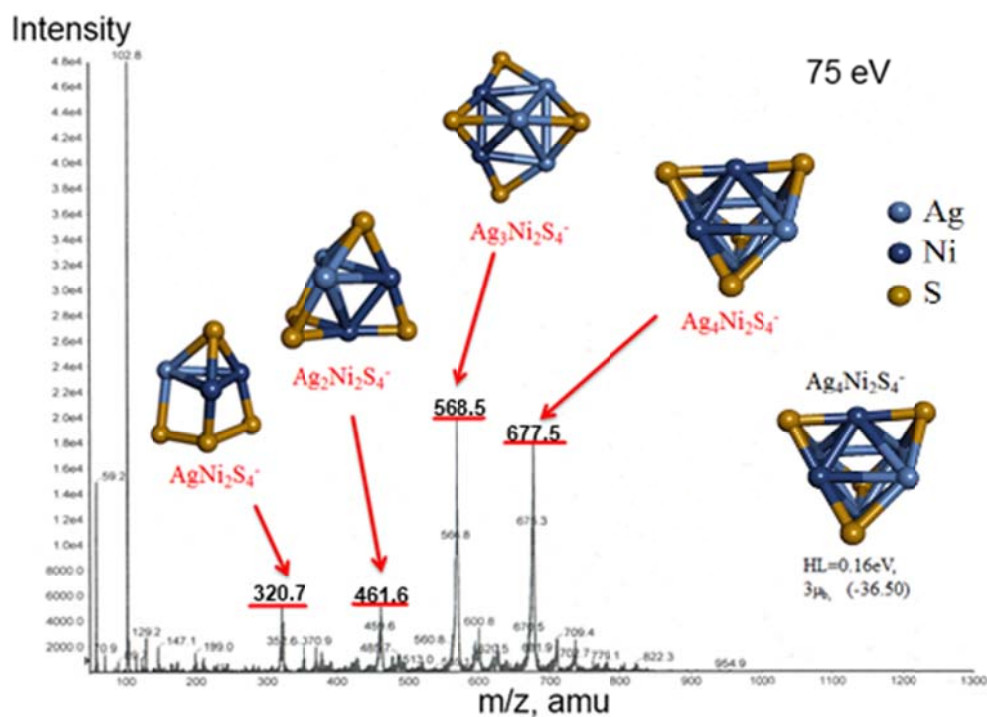
Figure 36. MS/MS of the $Ag_4Ni_2(DMSA)_4$ cluster using electrospray ionization MS at 75 eV, showing the ground state cluster geometries for the major peaks.
(MS/MS work done by collaborators in the A. Sen group at Pennsylvania State Univ.)

Chapter 5: Conclusions

To summarize our findings during the course of this work, the aforementioned theoretical, atomic and electronic structure calculations were performed using density functional theory to determine the structure and absorption spectra of the nanocluster $Ag_4Ni_2(DMSA)_4$. These results have indicated that cluster core of formula Ag_4Ni_2 forms a distorted octahedral structure with eight sulfurs occupy the vertices to form eight S-Ni and eight S-Ag bonds. The nanocluster is in the singlet ground state which tells us that the local magnetic moments of the nickel are quenched due to the bonding with sulfur and silver atoms, and thanks to this bonding, the cluster is extremely stable as displayed through its HOMO-LUMO gap of 1.28 eV. The quenched magnetic moments of the cluster were confirmed experimentally based on measurements collected using a superconducting quantum interface device (SQUID) that shows a very small magnetic moment, possibly due to contamination from extraneous nickel ions. The analysis of the local charges on various sites of the $Ag_4Ni_2(DMSA)_4$ cluster indicates that the stabilization occurs through charge transfer from the silver atoms to the $Ni(DMSA)_2$ complex, whose ground state electronic structure is in the triplet state. This stability is enhanced through addition of more silver atoms, each donating charge, but results in a closing of the electronic shell making the final cluster non-magnetic.

Studies of this kind into the energetics of fragments should be useful to identify any and all mechanisms that lead to the formation of a final motif. While we have concluded calculations

in regard to binding energies and electronic stability of neutral fragments and their anionic counterparts, the explication of results for this understanding is an ongoing process.

It is also advantageous to add that although the $Ag_4Ni_2(DMSA)_4$ cluster contains a surface with organics, there is still enough space for other molecules to approach the silver and sulfur atoms. These exposed sites offer yet another avenue of investigation to the functionality of ligand-protected nanoclusters containing a metal core. Thus, the resulting cluster material may be able to catalyze certain reactions. The information in regard to behavior of this type of cluster when used as a catalyst is limited or non-existent at this stage.   Even less is known of a bimetallic-cored analogue. These investigations will be taken on at a later date.

Bibliography & References

[1]   A. W. Castleman, S. N. Khanna, "Clusters, Superatoms, and Building Blocks of New Materials", *J. Phys. Chem.*, **113**, 2664 (2009)

[2]   S. A. Claridge, A. W. Castleman, S. N. Khanna, C. B. Murray, A. Sen, P. S. Weiss, "Cluster-Assembled Materials", *ACS NANO*, **3**, 244 (2009)

[3]   Y. Negishi, T. Iwai, M. Ide, "Continuous modulation of Electronic structure of stable thiolate-protected Au_{25} cluster by Ag doping", *Chem. Comm.*, **2010**, *2*, 2316-2321

[4]   C. A. Fields-Zinna, M. C. Crowe, A. Dass, J. E. F. Weaver, R. W. Murray, "Mass Spectrometry of Small Bimetal Monolayer-Protected Clusters", *Langmuir*, **2009**, *25*, 7704-7710

[5]   Z. Wu, E. Lanni, W. Chen, M. E. Bier, D. Ly, R. Jin, "High Yield, Large Scale Synthesis of Thiolate-Protected Ag_7 Clusters" ,*J. Am. Chem. Soc.*, **2009**, *131*, 16672-16674

[6]   H. Xiang, S. Wei, X. Gong, "Structures of $[Ag_7(SR)_4]^-$ and $[Ag_7(DMSA)_4]^-$", *J. Am. Chem. Soc.*, **2010**, *132*, 7355-7360

[7]   Szabo, Attila. Ostlund, Neil S, <u>Modern Quantum Chemistry: Introduction to Advanced Electronic Structure Theory</u>**.** New York, Macmillan Publishing 1982, McGraw-Hill 1989, Dover 1996. ISBN-13: 978-0-486-69186-2

Bibliography & References (Cont.)

[8]   Harrison, N. M, "An Introduction to Density Functional Theory", Appears in:

        Computational Materials Science, NATO Science Series III, Ed. Catlow and Kotomin,

        187, IOS Press, 2003

[9]   Parr, R. G, Yang, W, Density-Functional Theory of Atoms and Molecules, *International*

        Series of Monographs on Chemistry 16. New York. Oxford Univ. Press. 1989.

[10]   Eschrig, Helmut, The Fundamentals of DFT, Stuttgart. B.G. Teubner Verlagsgesellschaft.

        1996. ISBN: 3-8154-3030-5

[11]   Capelle, Klaus, "A Bird's-Eye View of Density-Functional Theory", 18 Nov. 2006,

        Version 5, arXiv:cond-mat/0211443v5, http://arxiv.org/abs/cond-mat/0211443

[12]   P. Hohenburg, W. Kohn, "Inhomogeneous Electron Gas", *Phys. Rev.*, **136**, B864, 1964

[13]   W. Koch, M. C. Holthausen, A Chemist's Guide to Density Functional Theory, 2ed.

        Wiley-VCH Verlag GmbH. 2001. ISBN: 3-527-30372-3

[14]   L. J. Sham, W. Kohn, "Self-Consistent Equations Including Exchange and Correlation

        Effects", *Phys. Rev. A.*, **140**, 4A, 1133-1138 (1965), doi:10.1103/PhysRev.140.A1133

[15]   G. te Velde, F. M. Bickelhaupt, E. J. Baerends, C. Fonseca Guerra,

        S. V. A. van Gisbergen, J. G. Snijders, T. Ziegler, "Chemistry with ADF", *J. Comput.*

        Chem., 2001, **23**, 931.

Bibliography & References (Cont.)

[16] J. P. Perdew, K. Burke, M. Ernzerhof, "Generalized Gradient Made Simple", *Phys. Rev. Lett.*, **77**, 8, 3865-3868

[17] R. M. Martin, Electronic Structure: Basic Theory and Practical Methods, New York. Cambridge University Press. 2004. ISBN: 978-0-521-53440-6

[18] Amsterdam Density Functional (ADF) Manual, Scientific Computing & Modeling NV, Vrije Universiteit, Theoretical Chemistry. Amsterdam, The Netherlands. 2013

[19] E. van Lenthe, E. J. Baerends, J. G. Snijders, "Relativistic regular two-component Hamiltonians", *J. Chem. Phys.*, **99**¸4597 (1993)

[20] E. van Lenthe, E. J. Baerends, J. G. Snijders, "Relativistic total energy using regular approximations", *J. Chem. Phys.*, **101**, 9783 (1994)

[21] E. van Lenthe, A. E. Ehlers, E. J. Baerends, "Geometry optimization in the Zero Order Regular Approximation for relativistic effects", *J. Chem. Phys.*, **110**, 8943 (1993)

[22] E. van Lenthe, J. G. Snijders, E. J. Baerends, "The zero-order regular approximation for relativistic effects: The effect of spin-orbit coupling in closed shell molecules", *J. Chem. Phys.*, **105**, 6505 (1996)

[23] E. van Lenthe, R. van Leeuwen, E. J. Baerends, J. G. Snijders, "Relativistic regular two-component Hamiltonians", *Int. Jour. Quant. Chem.*, **57**, 281 (1996)

Bibliography & References (Cont.)

[24]   S. R. Biltek, S. Mandal, A. Sen, A. C. Reber, A. F. Pedicini, S. N. Khanna,

"Synthesis and Structural Characterization of an Atom-Precise Bimetallic Nanocluster,

$Ag_4Ni_2(DMSA)_4$", *J. Am. Chem. Soc.*, 2013, 135, 26-29

[25]   F. W. McLafferty, "Molecular Rearrangements", *Anal. Chem.,* **31**, 1, 82-87 (Jan., 1959)

Vita

Anthony Filippo Pedicini was born on August 1, 1984, in Brooklyn, New York, and is an American citizen. He graduated from Meadowbrook High School, Chesterfield, Virginia in 2002. He received his Associates in Science from Richard Bland College, Petersburg, Virginia in 2005. He received his Bachelors of Science in Applied Mathematics and Bachelors of Science in Physics, with minor in Electrical Engineering, from Virginia Commonwealth University in 2011.

This page intentionally left blank.